Supplement of Atmos. Chem. Phys., 21, 18351–18374, 2021
https://doi.org/10.5194/acp-21-18351-2021-supplement

Atmospheric Chemistry and Physics
Open Access
EGU

Supplement of

Development and evaluation of a new compact mechanism for aromatic oxidation in atmospheric models

Kelvin H. Bates et al.

Correspondence to: Kelvin H. Bates (kelvin_bates@fas.harvard.edu)

Contents:

S1. Species and reactions in GC13

Table S1 lists the 17 unique species used in GC13 to simulate BTX chemistry, along with their chemical properties for implementation in GEOS-Chem. Henry's law coefficients are from Sander (2015) and Cabrera-Perez *et al.* (2016).[1,2] Table S2 lists species already in the GEOS-Chem mechanism that appear in the GC13 aromatic mechanism. Table S3 lists all reactions in GC13 that involve the species listed in Table S1. Finally, Tables S4 reactions for treatment of ethylbenzene, styrene, and trimethylbenzenes, as described in Section 5.4 of the main text.

Table S1: Unique species in GC13[a]

Name	Description	Formula	MW (g mol^{-1})	H[b] (M atm^{-1}) [K]
BENZ	Benzene	C_6H_6	78.11	1.8e-1 [4100]
TOLU	Toluene	C_7H_8	92.14	1.5e-1 [4000]
XYLE	Xylene	C_8H_{10}	106.18	1.7e-1 [4000]
ARO2*	Generic peroxy radical	$C_6H_7O_3$	127.12	—
PHENOL	Phenol	C_6H_6O	94.11	2.9e3 [6800]
CRESOL	Cresols and methylcresols	C_7H_8O	108.14	2.9e3 [6800]
CATECH	Catechols and methylcatechols	$C_7H_8O_2$	124.14	4.6e3 [0]
BZALD	Benzaldehyde and tolualdehyde	C_7H_6O	106.12	3.6e-1 [0]
BZCO3*	Acyl peroxy radical from BZALD	$C_7H_5O_3$	137.11	—
BZCO3H	(Methyl-) Perbenzoic acid	$C_7H_6O_3$	138.12	2.4e4 [0]
BENZP	Aromatic hydroperoxide	$C_6H_6O_2$	110.11	2.9e3 [6800]
BZPAN	(Methyl-) Peroxybenzoylnitrate	$C_7H_5O_5N$	183.12	7.0e1 [4600]
NPHEN	Nitrophenols and nitrocatechols	$C_6H_5O_3N$	139.11	7.0e1 [4600]
BENZO2*	Phenylperoxy radicals	$C_6H_5O_2$	109.10	—
BENZO*	Phenoxy radicals	C_6H_5O	93.10	—
AROMP4	Generic C4 intermediate	$C_4H_4O_2$	68.08	3.6e5 [7200]
AROMP5	Generic C5 intermediate	$C_5H_6O_2$	98.10	3.7e3 [7500]

[a]Radical species are denoted with *. [b]The first number denotes the Henry's Law coefficient (M atm^{-1}), while the second in brackets denotes its temperature dependence (Δ_{soln} H/R, in units K).

Table S2: Additional species in GC13

Name	Description	Formula	MW (g mol^{-1})	H[a] (M atm^{-1}) [K]
RCOOH	Generic C_{3+} carboxylic acids	$C_4H_8O_2$	88.11	—
RCHO	Generic C_{3+} aldehydes	C_4H_8O	72.11	4.2e3 [0]
RCO3	Generic C_{3+} acylperoxy radicals	$C_4H_9O_3$	105.11	—
R4O2	Generic C_{3+} peroxy radicals	$C_4H_9O_2$	89.11	—
R4N1	Generic C_{3+} nitrooxyperoxy radicals	$C_4H_8O_5N$	136.10	—
MVK	Methyl vinyl ketone	C_4H_6O	70.09	2.6e1 [4800]
MGLY	Methylglyoxal	$C_3H_4O_2$	72.06	3.7e3 [7500]
GLYX	Glyoxal	$C_2H_2O_2$	58.04	3.6e5 [7200]
MCO3	Acyl peroxy radical	$C_2H_3O_3$	75.04	—
GAOO	C_2 stabilized Criegee intermediate	$C_2H_4O_3$	76.05	—
ACTA	Acetic acid	$C_2H_4O_2$	60.05	4.1e3 [6300]

Table S2 cont'd

HCOOH	Formic acid	CH_2O_2	46.03	8.9e3 [6100]
MO2	Methyl peroxy radical	CH_3O_2	47.03	—
CH2O	Formaldehyde	CH_2O	30.03	3.0e3 [7200]
CO	Carbon monoxide	CO	28.01	9.7e-4 [1300]
CO2	Carbon dioxide	CO_2	44.01	—
O3	Ozone	O_3	48.00	1.9e-3 [1600]
HO2	Hydroxyl radical	HO_2	17.01	—
OH	Hydroperoxyl radical	HO	33.01	—
NO	Nitric oxide	ON	30.01	—
NO2	Nitrogen dioxide	O_2N	46.01	—
NO3	Nitrate radical	O_3N	62.00	—
HONO	Nitrous acid	HO_2N	47.01	—
HNO3	Nitric acid	HO_3N	63.01	8.3e4 [7400]

[a]The first number denotes the Henry's Law coefficient (M atm^{-1}), while the second in brackets denotes its temperature dependence (Δ_{soln} H/R, in units K).

Table S3: Reactions in GC13

Reactants	Products	Rate formula[a]	Ref.
BENZ + OH	0.54PHENOL + 0.54HO2 + 0.46ARO2 + 0.18GLYX + 0.08CO + 0.58AROMP4	Arr(2.3e-12,-193)	3
TOLU + OH	0.19CRESOL + 0.19HO2 + 0.81ARO2 + 0.06BZALD + 0.12GLYX + 0.12MGLY + 0.1CO + 0.35AROMP5 + 0.7AROMP4	Arr(1.8e-12,340)	3
XYLE + OH	0.15CRESOL + 0.15HO2 + 0.85ARO2 + 0.06BZALD + 0.1GLYX + 0.2MGLY + 0.12CO + 0.6AROMP5 + 0.3AROMP4 + 0.47RCOOH	Arr(1.7e-11,0)	3
ARO2 + HO2	OH + HO2	Arr(2.39e-13,1300)	4,5
ARO2 + NO	NO2 + HO2	Arr(2.6e-12,365)	4,5
ARO2 + NO3	NO2 + HO2	Arr(2.3e-12,0)	4,5
ARO2 + MO2	CH2O + 2.0HO2	Arr(1.7e-13,220)	4,5
ARO2 + MCO3	MO2 + HO2	Arr(4.2e-13,220)	4,5
PHENOL + OH	0.06BENZO + 0.06GLYX + 0.18AROMP4 + 0.14ARO2 + 0.8CATECH + 0.8HO2	Arr(4.7e-13,1220)	3-5
PHENOL + NO3	0.258NPHEN + 0.742HNO3 + 0.742BENZO	Arr(3.8e-12,0)	3-5
CRESOL + OH	0.727CATECH + 0.727HO2 + 0.2ARO2 + 0.073BENZO + 0.3AROMP4 + 0.2AROMP5	Arr(2.0e-12,970)	3-5
CRESOL + NO3	0.5NPHEN + 0.2ARO2 + 0.5HNO3 + 0.3BENZO + 0.3AROMP4 + 0.2AROMP5	Arr(1.25e-11,0)	3-5
CATECH + OH	0. 3BENZO + 0.7ARO2 + 1.05AROMP4	Arr(1.5e-11,0)	3-6
CATECH + O3	GAOO + HO2 + OH + AROMP4	Arr(9.2e-18,0)	4,5
CATECH + NO3	0.5NPHEN + 0.5HNO3 + 0.3BENZO + 0.2ARO2 + 0.3AROMP4	Arr(9.9e-11,0)	3-5
BZALD	BENZO2 + CO + HO2	3.7e-4 × j_{NO2}	3,7
BZALD + OH	BZCO3	Arr(5.9e-12,225)	3-5

Table S3 cont'd

BZALD + NO3	BZCO3 + HNO3	Arr(2.4e-15,0)	4,5
BZCO3 + HO2	0.35CO2 + 0.2BENZO2 + 0.15O3 + 0.2OH + 0.15BENZP + 0.65BZCO3H	Arr(1.1e-11,340)	8
BZCO3 + NO	NO2 + CO2 + BENZO2	Arr(7.5e-12,290)	4,5
BZCO3 + NO2	BZPAN	PAN(3.28e-28, -6.87,0,1.125e-11, -1.105,0)	4,5
BZCO3 + MO2	BENZO2 + CO2 + HO2 + CH2O	Arr(2.67e-12,365)	4,5
BZCO3H + OH	BZCO3	Arr(4.66e-12,0)	4,5
BZCO3H	BENZO2 + OH + CO2	4.5e-4 × j_{NO2}	4,5,9
BZPAN	BZCO3 + NO2	PAN(1.10e-5,0, -10100,1.90e17,0, -14100,)×0.67	4,5
BZPAN + OH	BENZP + CO2 + NO2	Arr(1.06e-12,0)	4,5
BENZO2 + NO2	BENZO + NO3	Arr(7.0e-12,0)	10
BENZO2 + NO	BENZO + NO2	Arr(2.67e-12,365)	4,5
BENZO2 + NO3	BENZO + NO2	Arr(2.30e-12,0)	4,5
BENZO2 + HO2	BENZOP	Arr(2.24e-13,1300)	4,5
BENZO2 +MO2	BENZO + HO2 + CH2O	Arr(1.7e-13,220)	4,5
BENZP + OH	BENZO2	Arr(3.60e-12,0)	4,5
BENZP	BENZO + OH	6.5e-4 × j_{NO2}	4,5,9
BENZO + O3	BENZO2	Arr(2.86e-13,0)	11
BENZO + NO2	NPHEN	Arr(2.08e-12,0)	12
NPHEN	HONO + CO + CO2 + AROMP4 + HO2	1.3e-3 × j_{NO2}	13,14
NPHEN + OH	0.5R4N1 + AROMP4 + 0.5NO2	Arr(3.47e-12,0) [b]	4,5,9
NPHEN + NO3	0.5HNO3 + NO2 + 0.5R4N1 + AROMP	Arr(2.60e-12,0) [b]	4,5,9
AROMP4 + OH	0.6GLYX + 0.25CO + 0.25HCOOH + 0.25OH + 0.33HO2 + 0.33RCO3 + 0.45RCOOH	Arr(5.5e-11,0)	15,16
AROMP4 + O3	0.5HCOOH + 0.6CO + GLYX + 0.4GAOO + 0.1HO2 + 0.1OH +0.1CO2	Arr(9.0e-16,0)	15,16
AROMP4	0.25HO2 + 0.25RCO3 + 0.25CO + RCHO	Arr(8.5e-4,0)	15,16
AROMP5 + OH	0.6MGLY + 0.15ACTA + 0.1HCOOH + 0.25OH + 0.33HO2 + 0.33RCO3 + 0.25CO + 0.52RCOOH	Arr(5.5e-11,0)	15,16
AROMP5 + O3	MGLY + 0.3ACTA + 0.2HCOOH + 0.6CO + 0.1CO2 + 0.25GAOO + 0.1HO2 + 0.1OH	Arr(9.0e-16,0)	15,16
AROMP5	0.4HO2 + 0.25R4O2 + 0.4CO + 0.15MVK + RCHO	Arr(8.5e-4,0)	15,16

[a]Arr. = Arrhenius; PAN = three-body pressure-dependent rate. Photolysis reactions are written as a scaling of j_{NO2}. (X,Y) for "Arr." reactions computes as $k = X \times e^{(Y/T)}$, where T represents temperature (K); (U,V,W,X,Y,Z) for "PAN" reactions computes as A×B×(10^(-0.523/(1+(log$_{10}$(A/B)/(1.414))^2)))/(A+B), where A = Arr(U,V)×(T/300)^W, B = Arr(X,Y)×(T/300)^Z, T = temperature (K), and [M] = the local number density of air (molecules cm^{-3}). Unimolecular rates are in units s^{-1}, while bimolecular rates have units cm^3 molecule^{-1} s^{-1}; [b]reaction rates for NPHEN are derived from nitrocatechols.

Table S4: Reactions of styrene (STY), ethylbenzene (EBZ), and trimethylbenzenes (TMB)[a]

Reactants	Products	Rate constant
STY + OH	ARO2 + HO2 + CH2O + BZALD	5.8×10^{-11}
STY + O3	0.5SCI[b] + 0.5CH2O + 0.62BZALD + 0.1BENZ + 0.28BENZO2 + 0.18CO + 0.18OH + 0.1HO2	1.7×10^{-17}
STY + NO3	ARO2 + NO2 + CH2O + BZALD	1.5×10^{-12}
EBZ + OH	0.82ARO2 + 0.25CH2O + 0.07BZALD + 0.18CRESOL + 0.4ALD2[c] + 0.4AROMP5 + 0.8AROMP4 + 0.18HO2	7.0×10^{-12}
EBZ + NO3	ARO2 + HNO3+ CH2O + BZALD	1.2×10^{-16}
TMB + OH	0.97ARO2 + 0.12CH2O + 0.05BZALD + 0.03CRESOL + 0.75AROMP5 + 0.375AROMP4 + 0.25MGLY + 0.1GLYX + 0.5RCOOH + 0.12CO + 0.03HO2	3.92×10^{-11}
TMB + NO3	ARO2 + HNO3 + 0.4AROMP5 + BZALD	1.4×10^{-15}

[a]These reactions are not included in GC13 as implemented in the main text, but are provided for future implementation, and are derived from MCM;[4,5] [b]SCI refers to the C_1 stabilized Criegee intermediate already included in the GEOS-Chem mechanism; [c]ALD2 refers to acetaldehyde.

S2. Additional product yields from chamber oxidation of benzene, toluene, and xylene

Figures S1-2 show measured and modeled yields of epoxides, photolabile dicarbonyls, formic acid, and acetic acid from individual aromatic precursors during the initial stages of chamber oxidation. Figures S3-5 are analogous to Figures 5-6 in the main text and Figure S2, but show yields after 24 hours of chamber oxidation rather than initial yields.

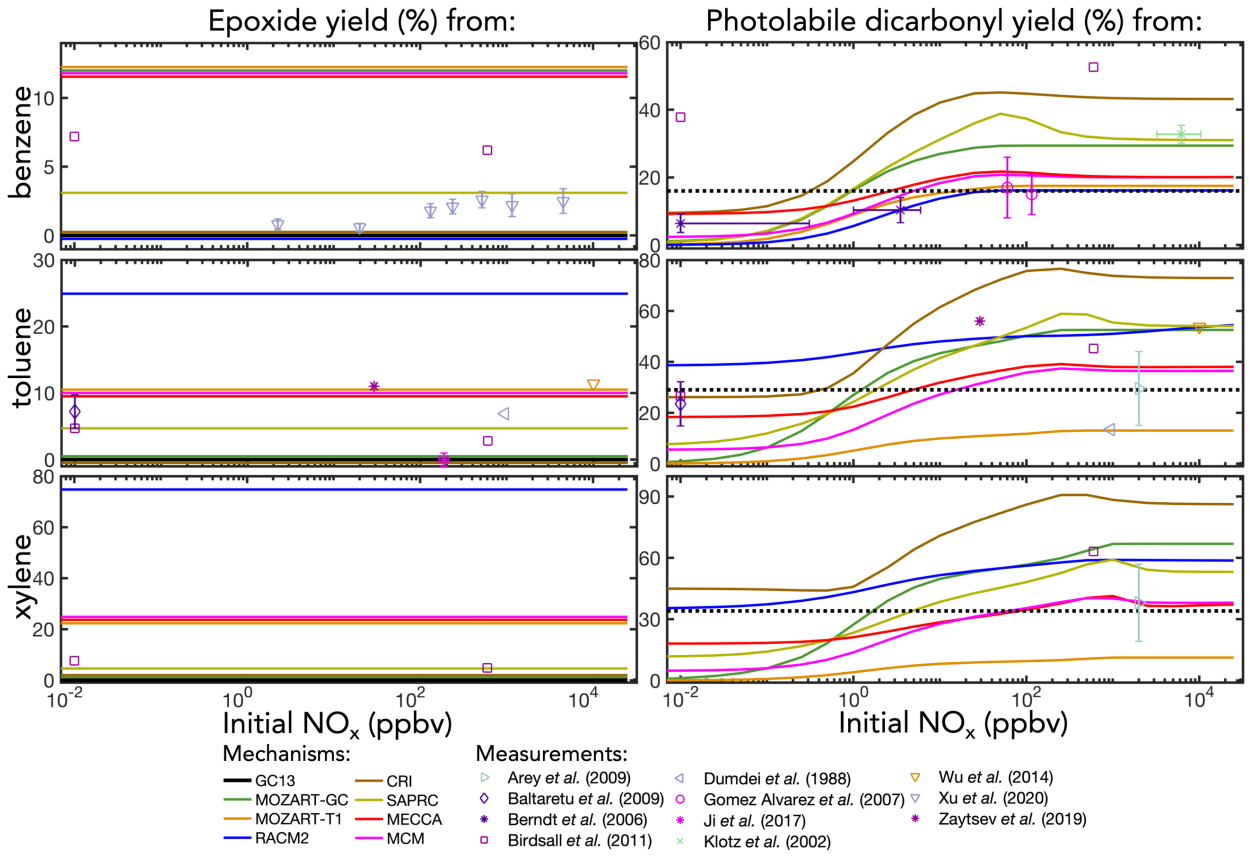

Figure S1. Experimental and simulated early yields of ring-opened epoxides (left) and photolabile dicarbonyls (right, including biacetyl and conjugated dicarbonyls) from benzene, toluene, and xylene oxidation as a function of initial NOx mixing ratio. GC13 does not include epoxides, and does not explicitly represent photolabile dicarbonyls, instead lumping them with other intermediates. The implicit photolabile dicarbonyl yield in GC13, treated as a fraction of the initial yield of the lumped intermediates, is shown in the dashed black line.

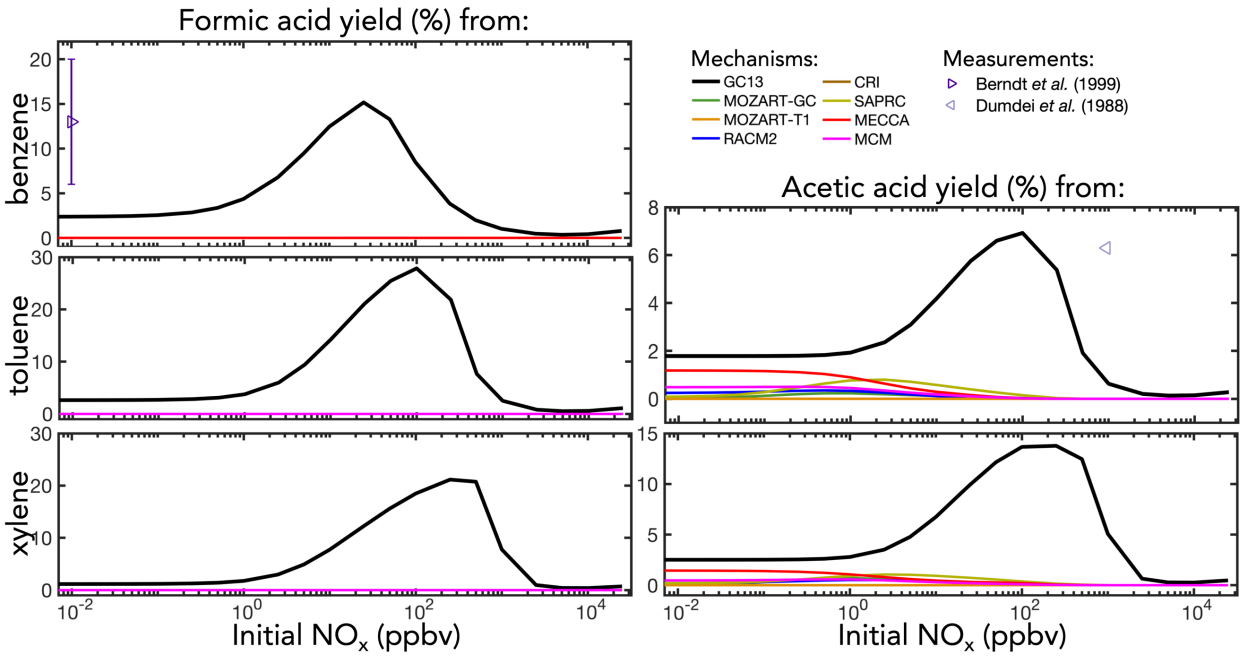

Figure S2. Experimental and simulated early yields of formic and acetic acids from benzene, toluene, and xylene oxidation as a function of initial NOx mixing ratio.

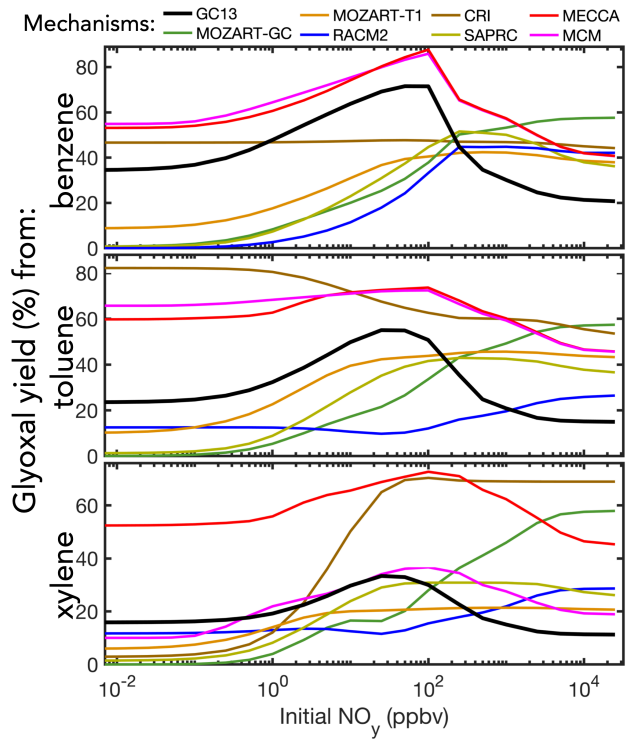

Figure S3. Simulated long-term chamber yields of glyoxal from benzene, toluene, and xylene oxidation as a function of initial NOx mixing ratio after 24 hours of oxidation, from simulations initialized with initial VOC mixing ratios of 10 ppb.

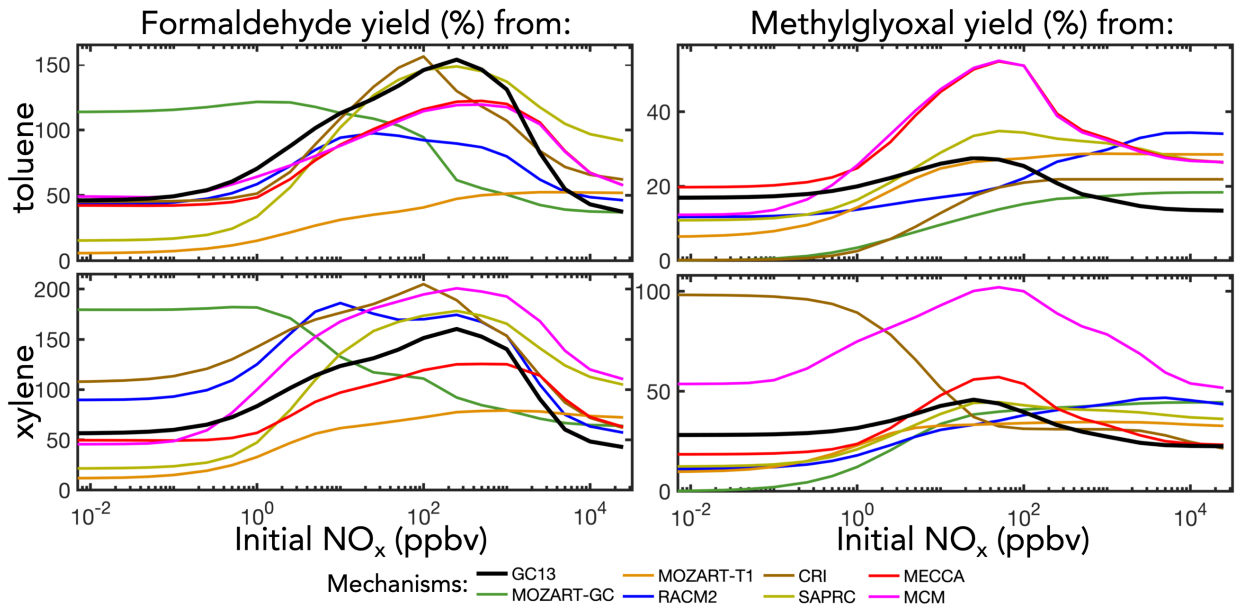

Figure S4. Simulated long-term chamber yields of methylglyoxal and formaldehyde from toluene and xylene oxidation as a function of initial NOx mixing ratio after 24 hours of oxidation, from simulations initialized with initial VOC mixing ratios of 10 ppb.

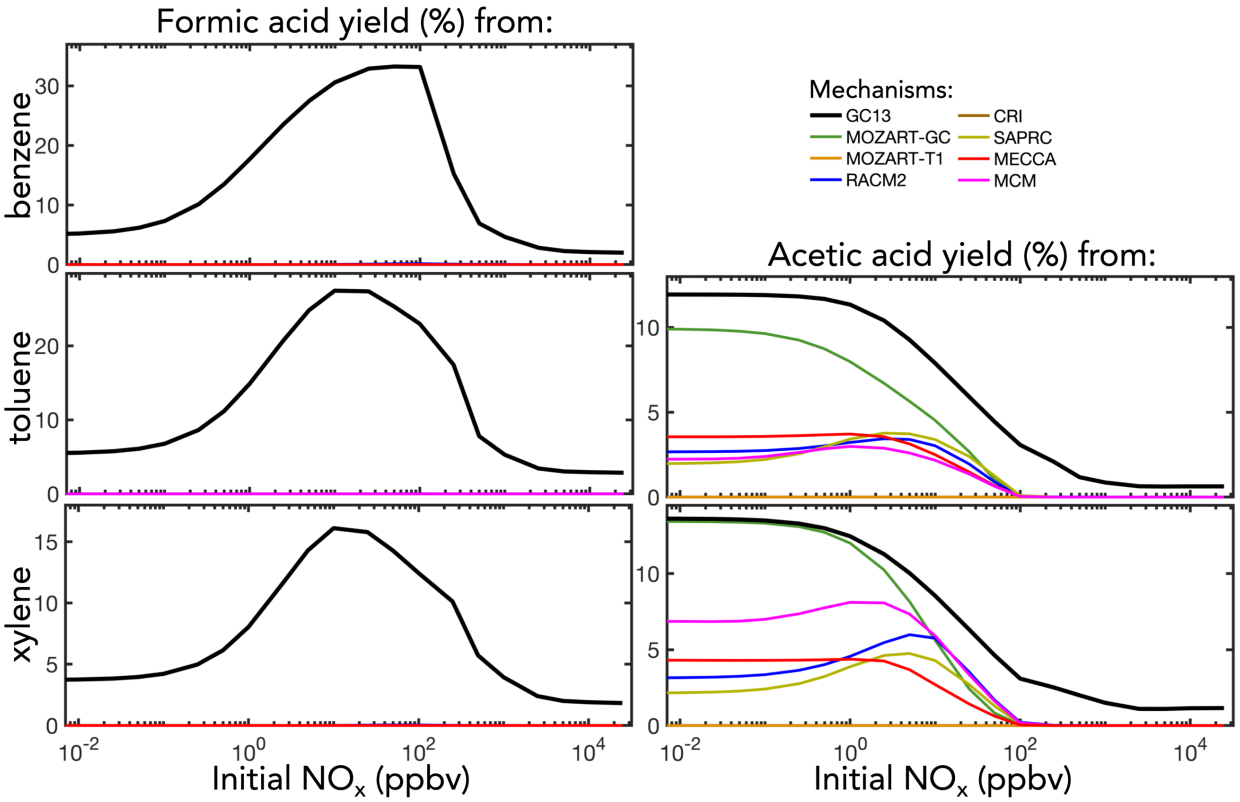

Figure S5. Simulated long-term chamber yields of formic and acetic acids from benzene, toluene, and xylene oxidation as a function of initial NOx mixing ratio after 24 hours of oxidation, from simulations initialized with initial VOC mixing ratios of 10 ppb.

S3. Precursor-specific simulations of ambient benzene, toluene, and xylene oxidation

Figures S6-S7 are analogous to Figures 7-8 in the main text, but show the effects of individual aromatic precursors instead of the mixed emissions. Figure S8 shows the glyoxal-to-formaldehyde ratio from mixed aromatic emissions, toluene, and xylene (as benzene has near-zero formaldehyde yields).

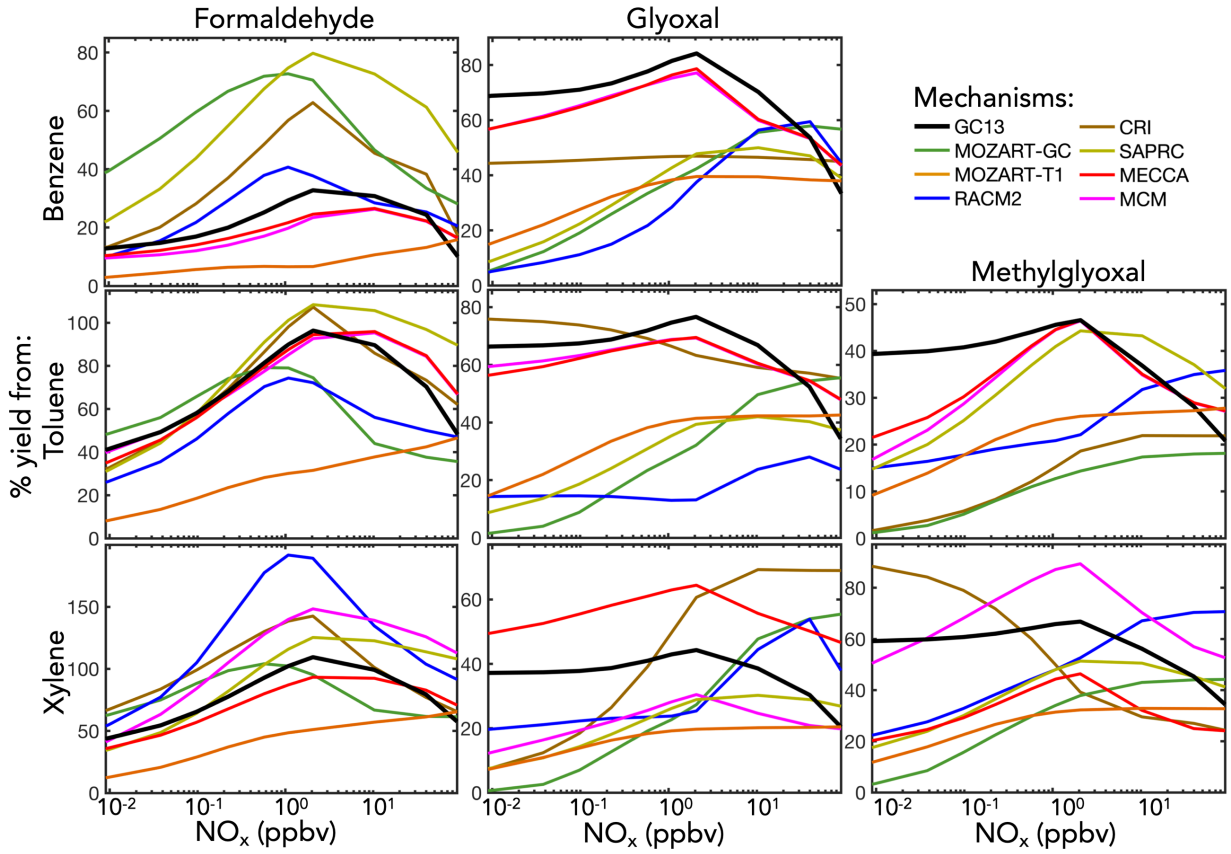

Figure S6. Simulated molar yields of formaldehyde, glyoxal, and methylglyoxal from separate benzene, toluene, and xylene oxidation in a continental boundary layer as a function of midday NO_x mixing ratio. Model setup is described in Section 4.1. Molar yields are averaged over the 8th simulated day.

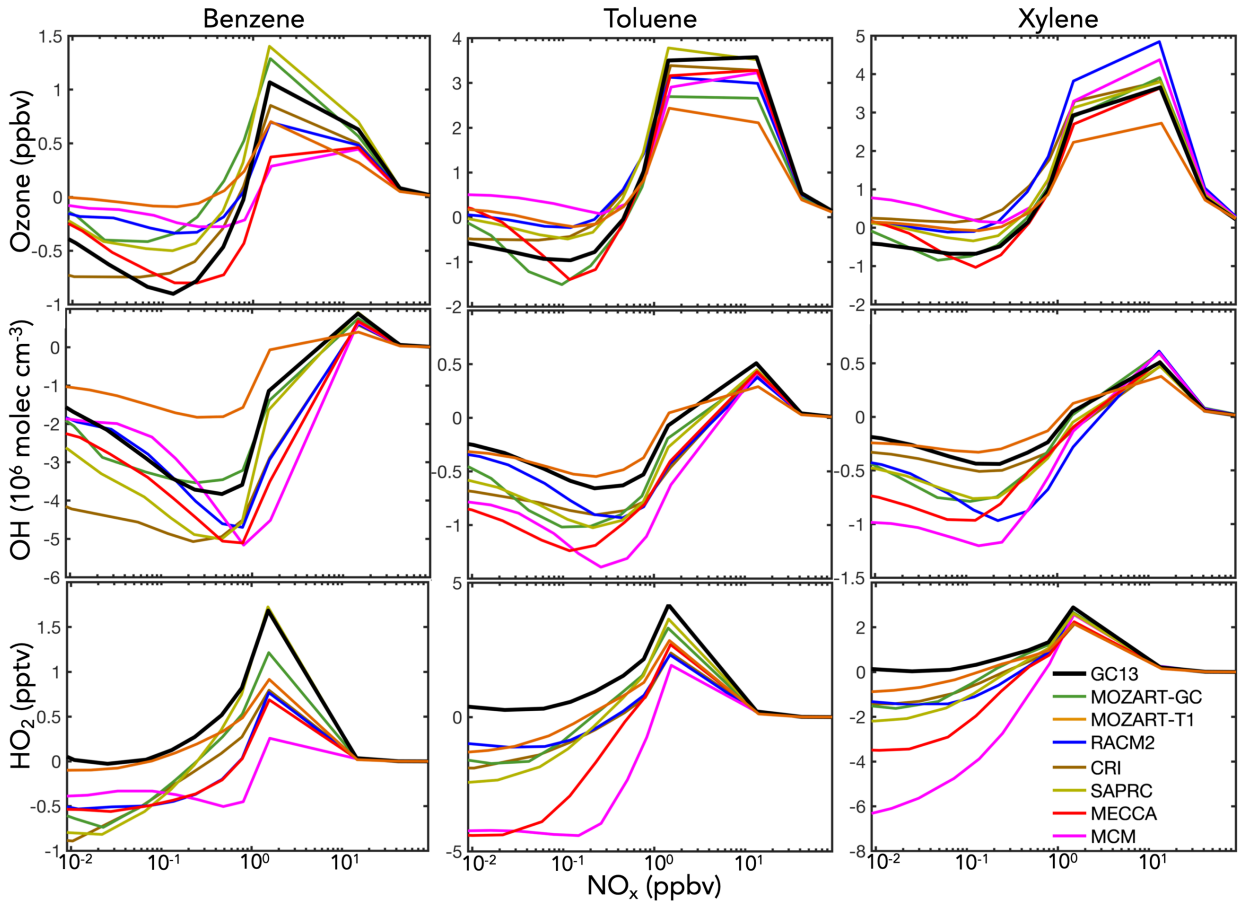

Figure S7: Changes in ozone, OH, and HO_2 due to aromatic chemistry with individual aromatic precursors in box model simulations of the continental boundary layer. Changes in species concentrations are calculated by subtracting midday (10:00-14:00) mean values in a simulation without aromatic emissions from those in an equivalent simulation with aromatic emissions, and are plotted against midday NO_x mixing ratio. Model setup is described in Section 4.1.

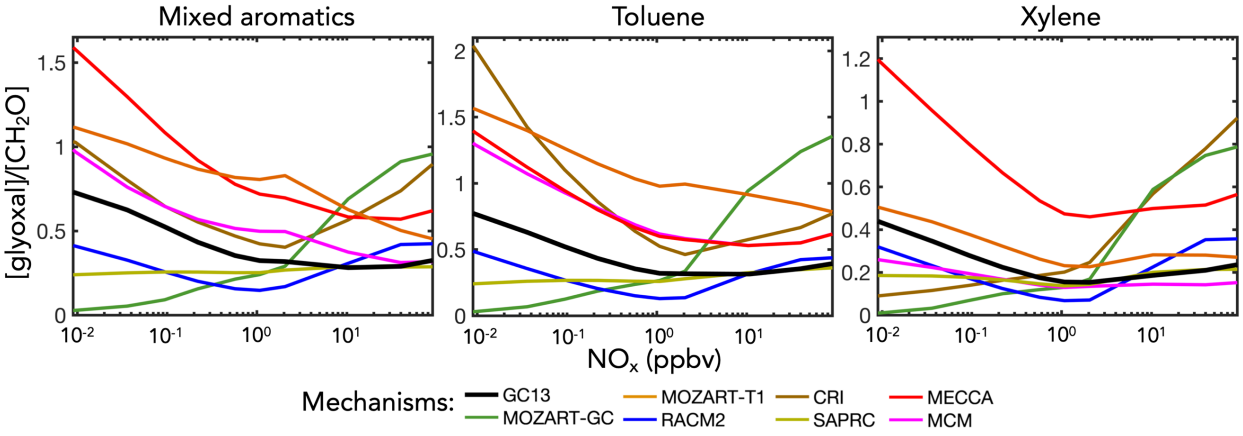

Figure S8. Midday (10:00-14:00) mean glyoxal-to-formaldehyde concentration ratios from oxidation of mixed aromatics (left), toluene (middle), and xylene (right) in box model simulations of the continental boundary layer as a function of midday NO_x mixing ratio. Model setup is described in Section 4.1.

S4. Sensitivities of box model results to temperature, $[VOC]_0$-, and other parameters

Figures S9-S14 show the temperature sensitivity of short- and long-term chamber yields of key VOC products from benzene, toluene, and xylene oxidation in each aromatic mechanism. In general, the mechanisms exhibit minimal temperature dependence, with the long-term yields of formaldehyde from toluene and xylene (which increase at higher temperatures and decrease at lower temperatures) as the only exception (Figure S13).

Figures S15-S24 show analogous sensitivities to initial aromatic VOC concentrations (for chamber simulations) or rates of VOC emissions (for ambient simulations) rather than temperature. While few mechanisms (only CRI, MECCA, and MCM) include explicit RO_2-RO_2 chemistry for aromatic peroxy radicals, all mechanisms exhibit similar sensitivities to VOC concentrations or emission rate. In chamber simulations, formaldehyde yields from toluene and xylene and glyoxal and formic acid yields from benzene are most sensitive to initial VOC concentration.

Finally, Figures S25-S26 show the sensitivities of short- and long-term chamber yields of key VOC products from benzene, toluene, and xylene oxidation in in GC13 to $[H_2O_2]_0$ and light flux.

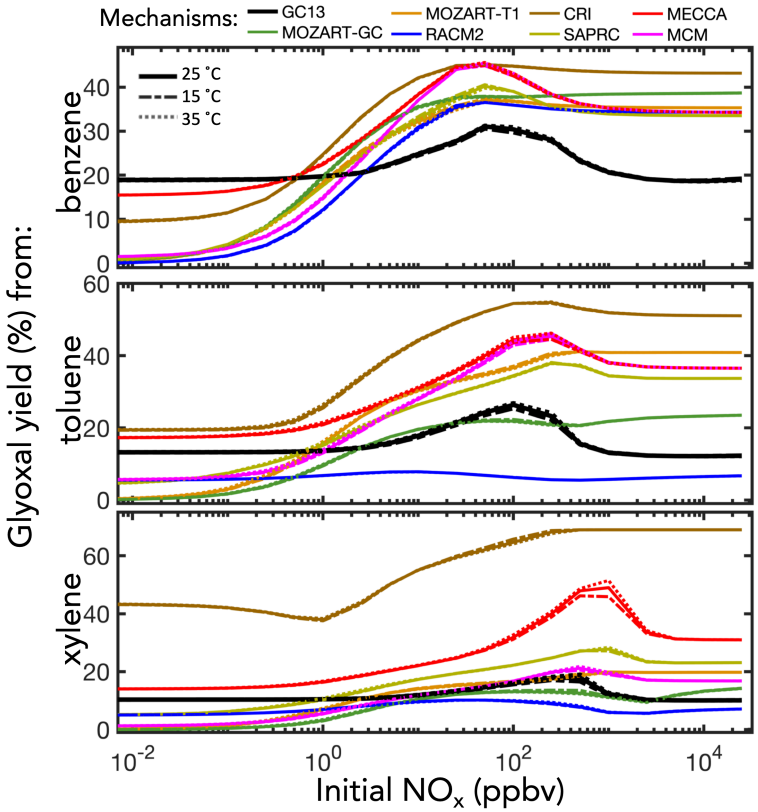

Figure S9. Like Figure 5 in the main text, but showing results for simulations at different temperatures in patterned lines.

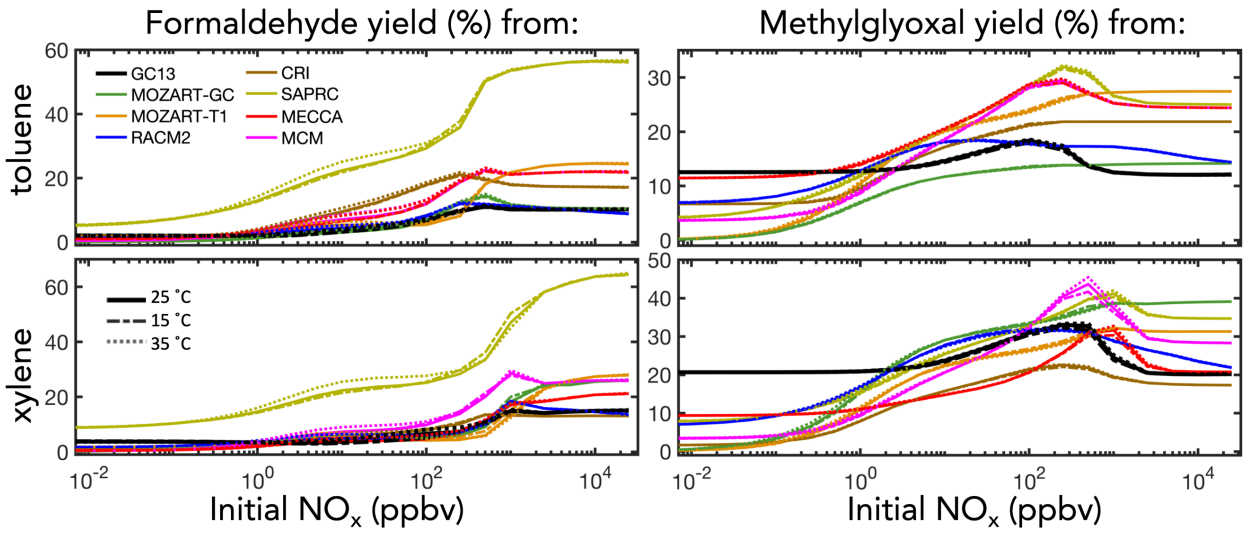

Figure S10. Like Figure 6 in the main text, but showing results for simulations at different temperatures in patterned lines.

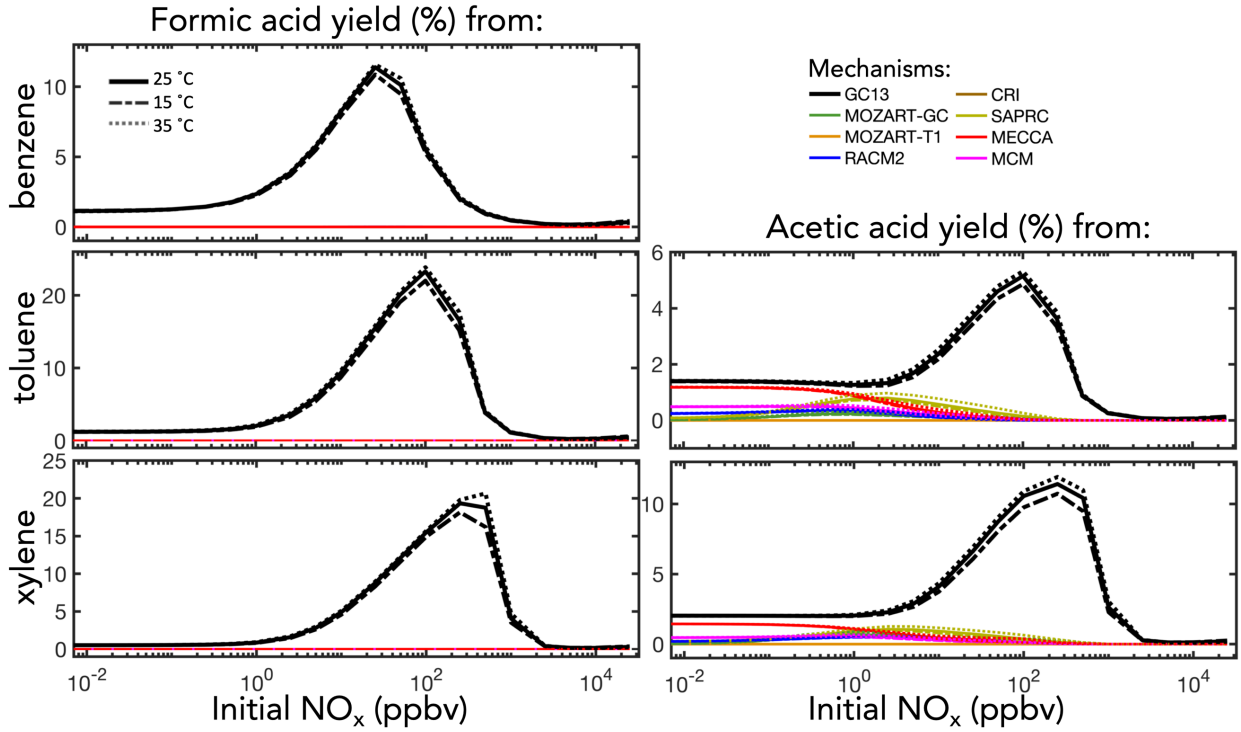

Figure S11. Like Figure S2, but showing results for simulations at different temperatures in patterned lines.

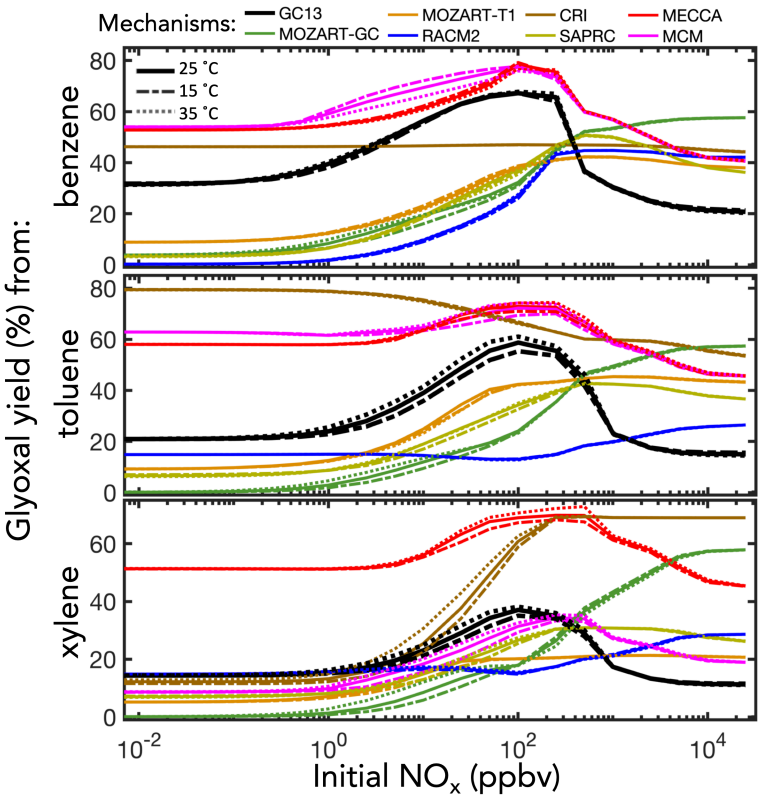

Figure S12. Like Figure S3, but showing results for simulations at different temperatures in patterned lines.

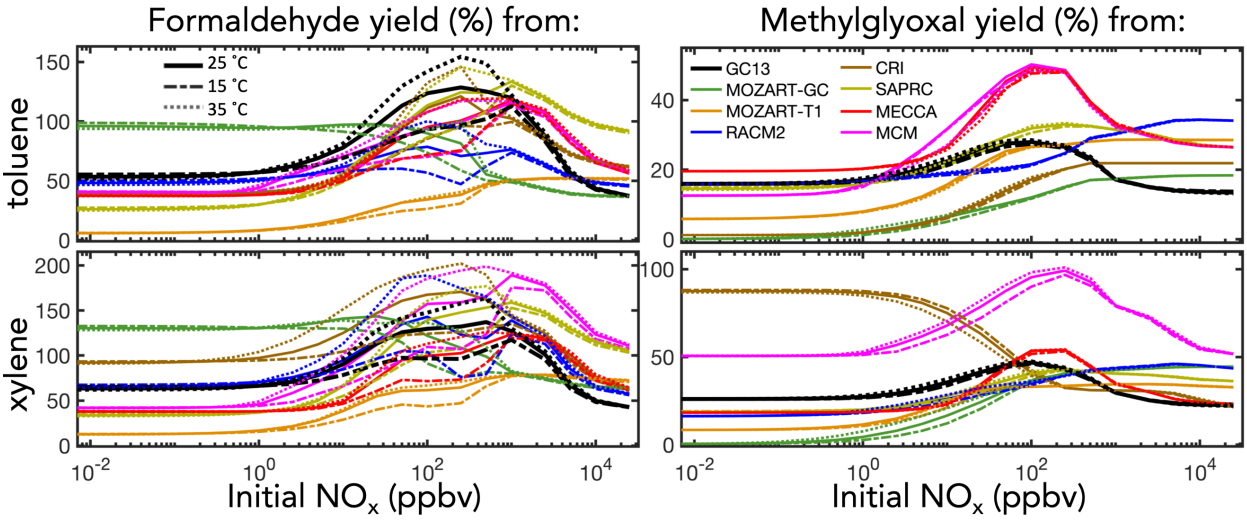

Figure S13. Like Figure S4, but showing results for simulations at different temperatures in patterned lines.

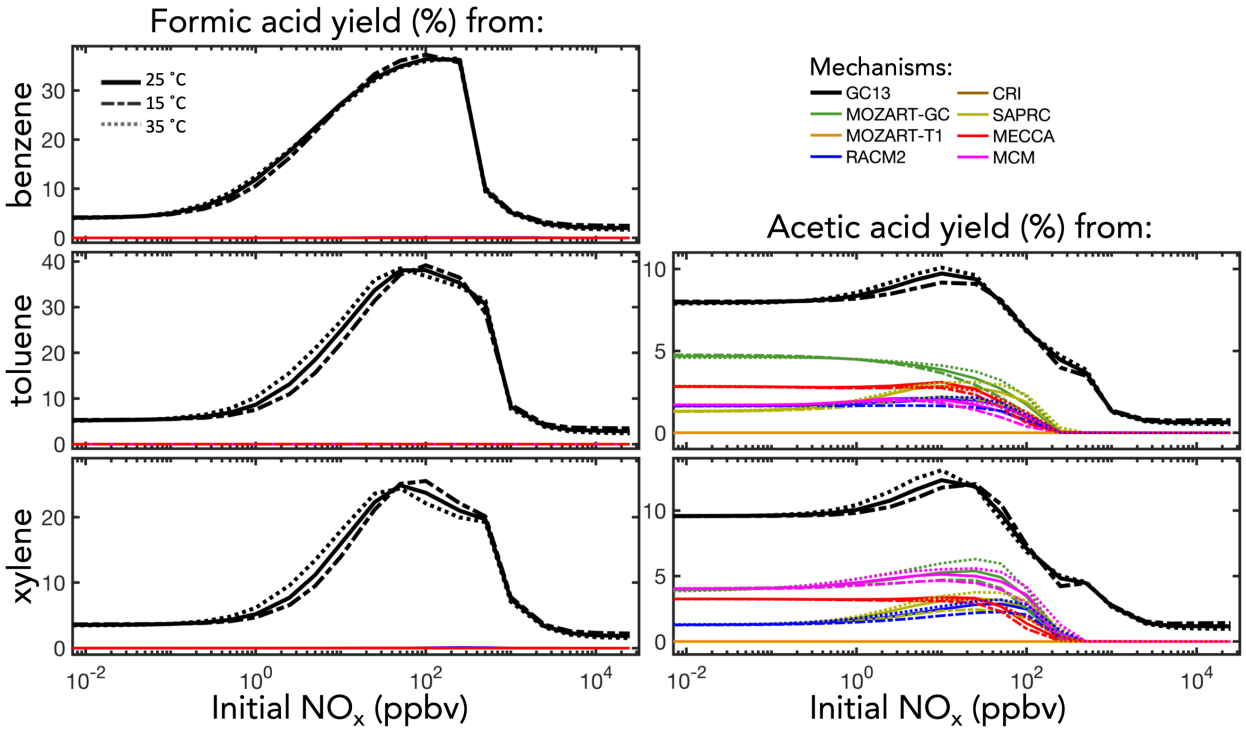

Figure S14. Like Figure S5, but showing results for simulations at different temperatures in patterned lines.

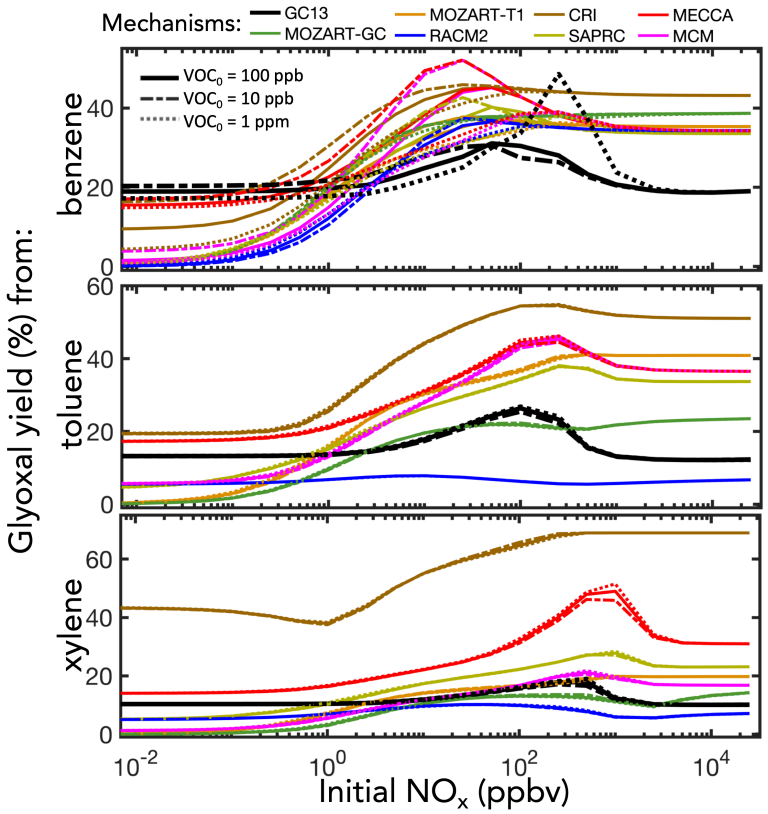

Figure S15. Like Figure 5 in the main text, but showing results for simulations with different initial aromatic VOC concentrations in patterned lines.

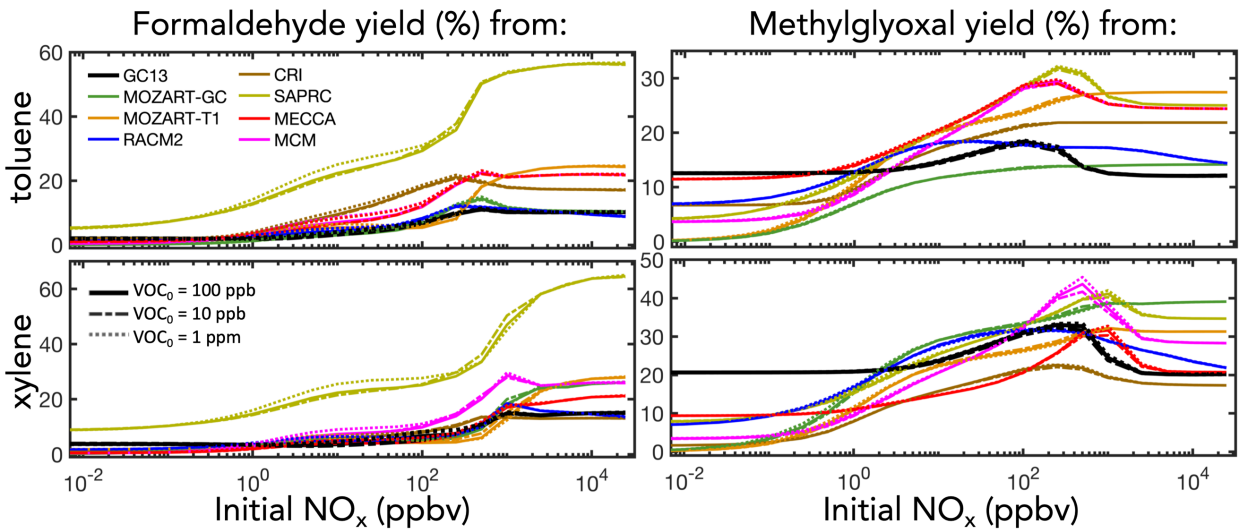

Figure S16. Like Figure 6 in the main text, but showing results for simulations with different initial aromatic VOC concentrations in patterned lines.

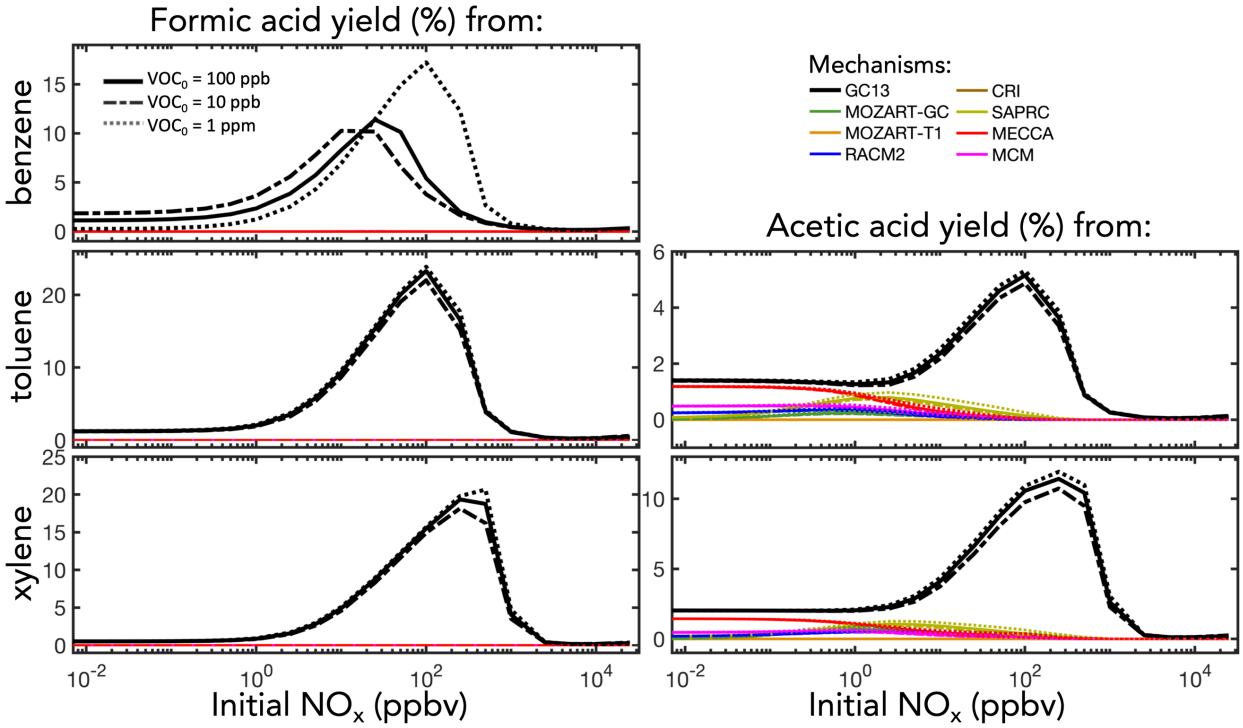

Figure S17. Like Figure S2, but showing results for simulations with different initial aromatic VOC concentrations in patterned lines.

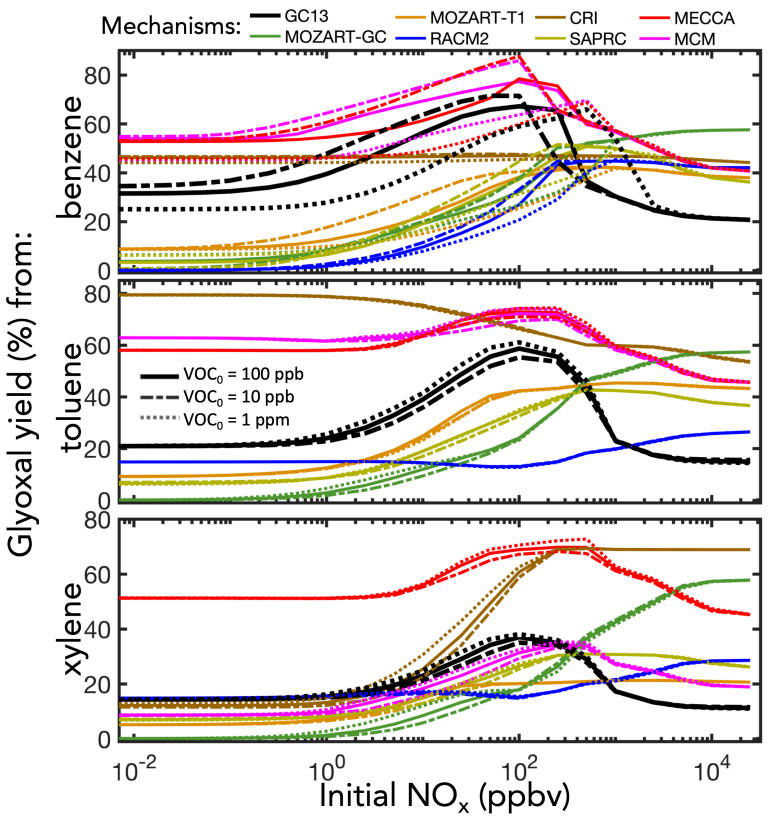

Figure S18. Like Figure S3, but showing results for simulations with different initial aromatic VOC concentrations in patterned lines.

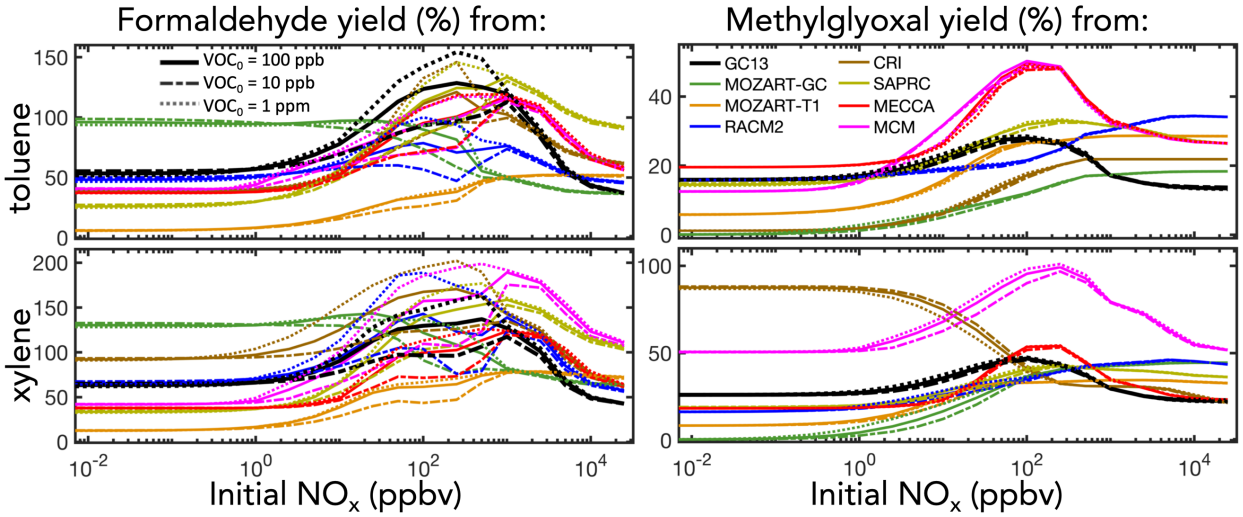

Figure S19. Like Figure S4, but showing results for simulations with different initial aromatic VOC concentrations in patterned lines.

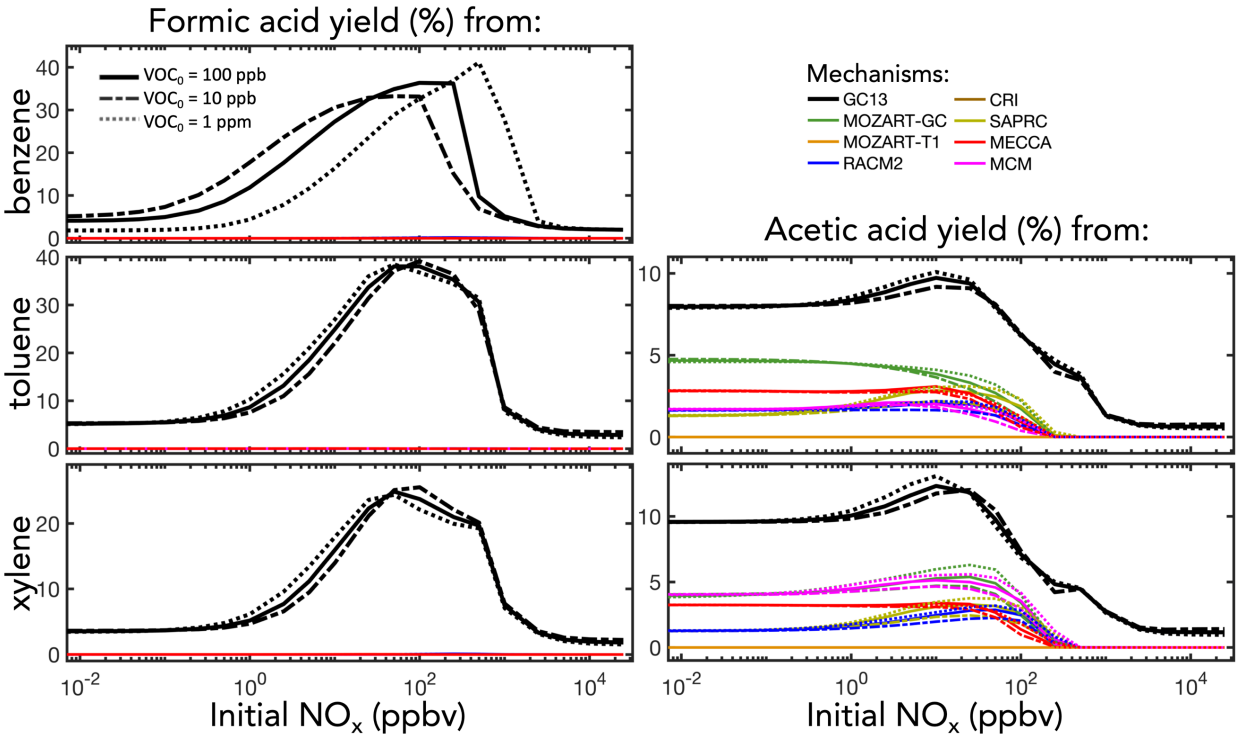

Figure S20. Like Figure S5, but showing results for simulations with different initial aromatic VOC concentrations in patterned lines.

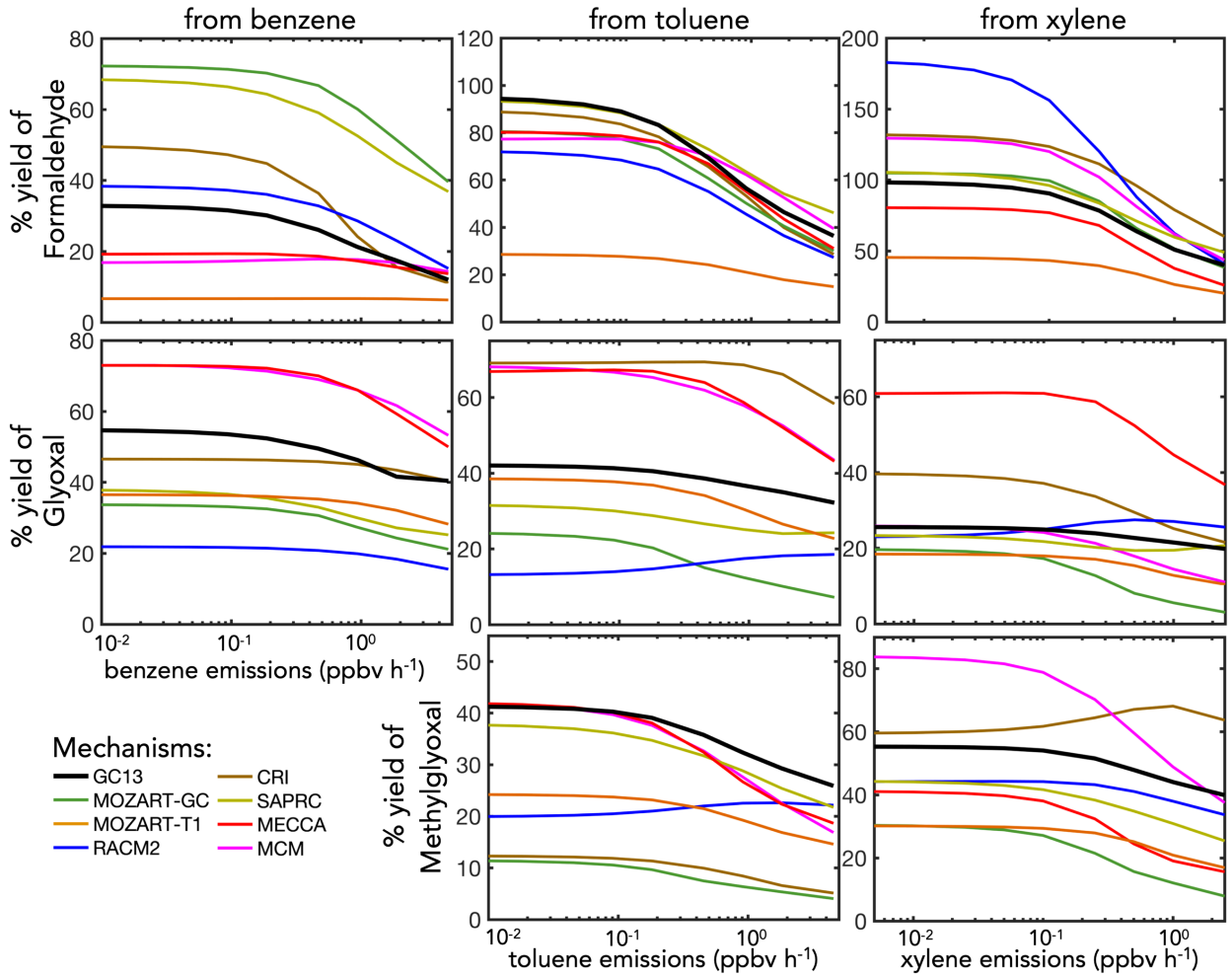

Figure S21. Like Figure S6, but plotting product yields against VOC emission rate rather than against NO emission rate, for a fixed NO emission rate of 100 ppt h^{-1}, corresponding to a midday NO_x mixing ratio of ~400 ppt.

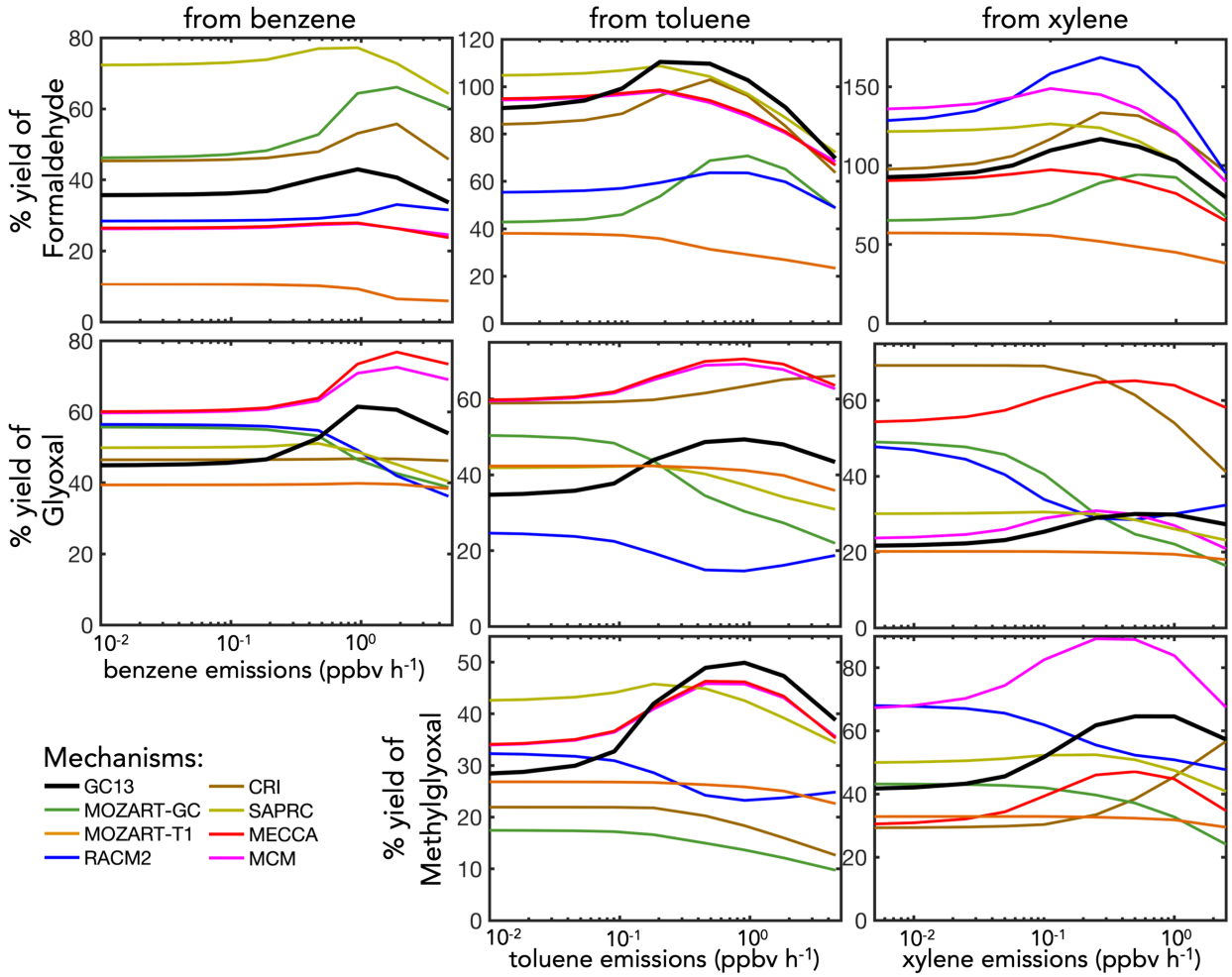

Figure S22. Like Figure S21, but at a higher fixed NO emission rate of 1 ppb h^{-1}, corresponding to a midday NO_x mixing ratio of ~7 ppb.

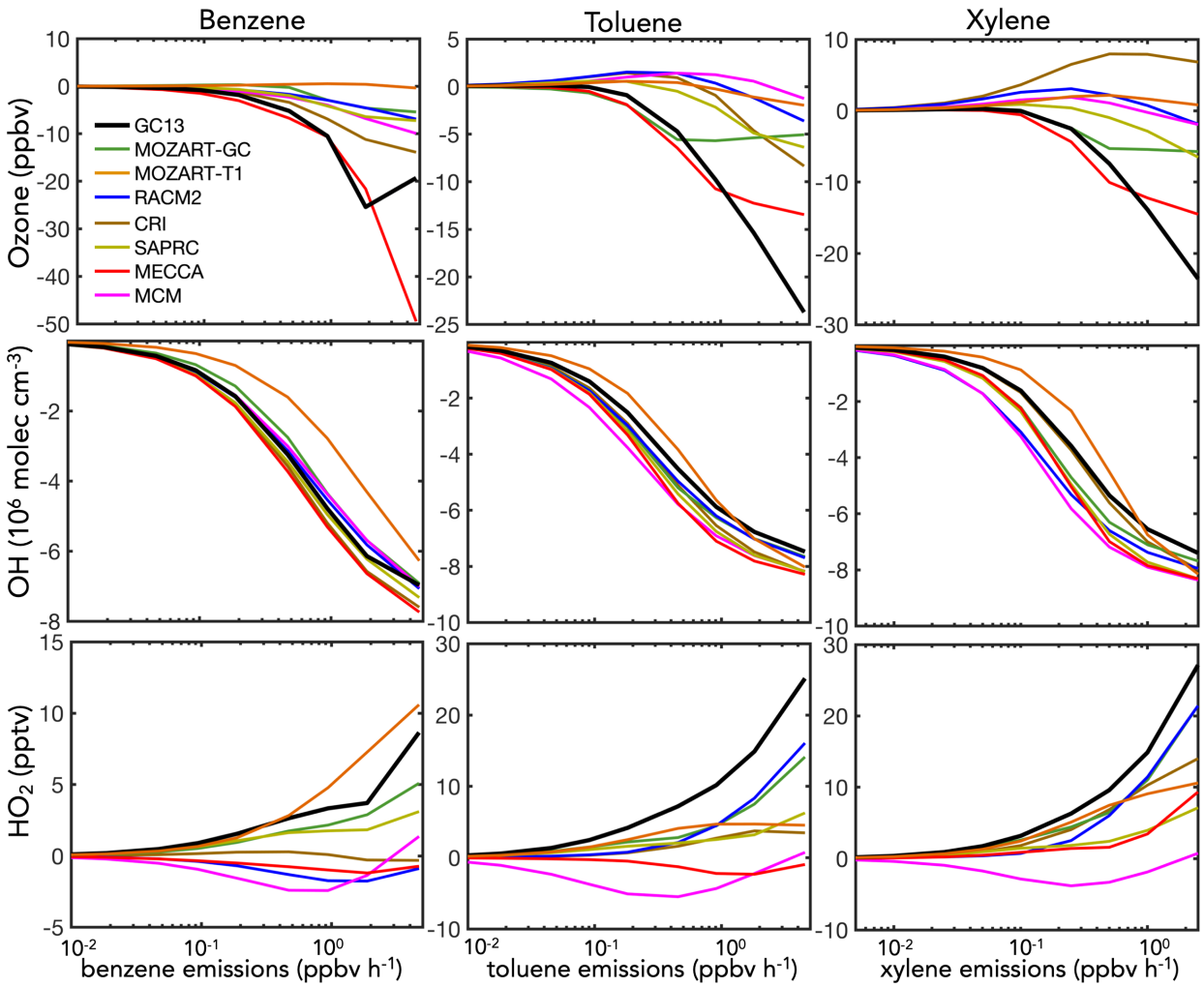

Figure S23. Like Figure S7, but plotting effects on ozone and HO_x against VOC emission rate rather than against NO emission rate, for a fixed NO emission rate of 100 ppt h^{-1}, corresponding to a midday NO_x mixing ratio of ~400 ppt. Changes in OH, HO_2, and ozone concentrations are calculated by subtracting their midday (10:00-14:00) mean values in a simulation without aromatic emissions from those in an equivalent simulation with aromatic emissions.

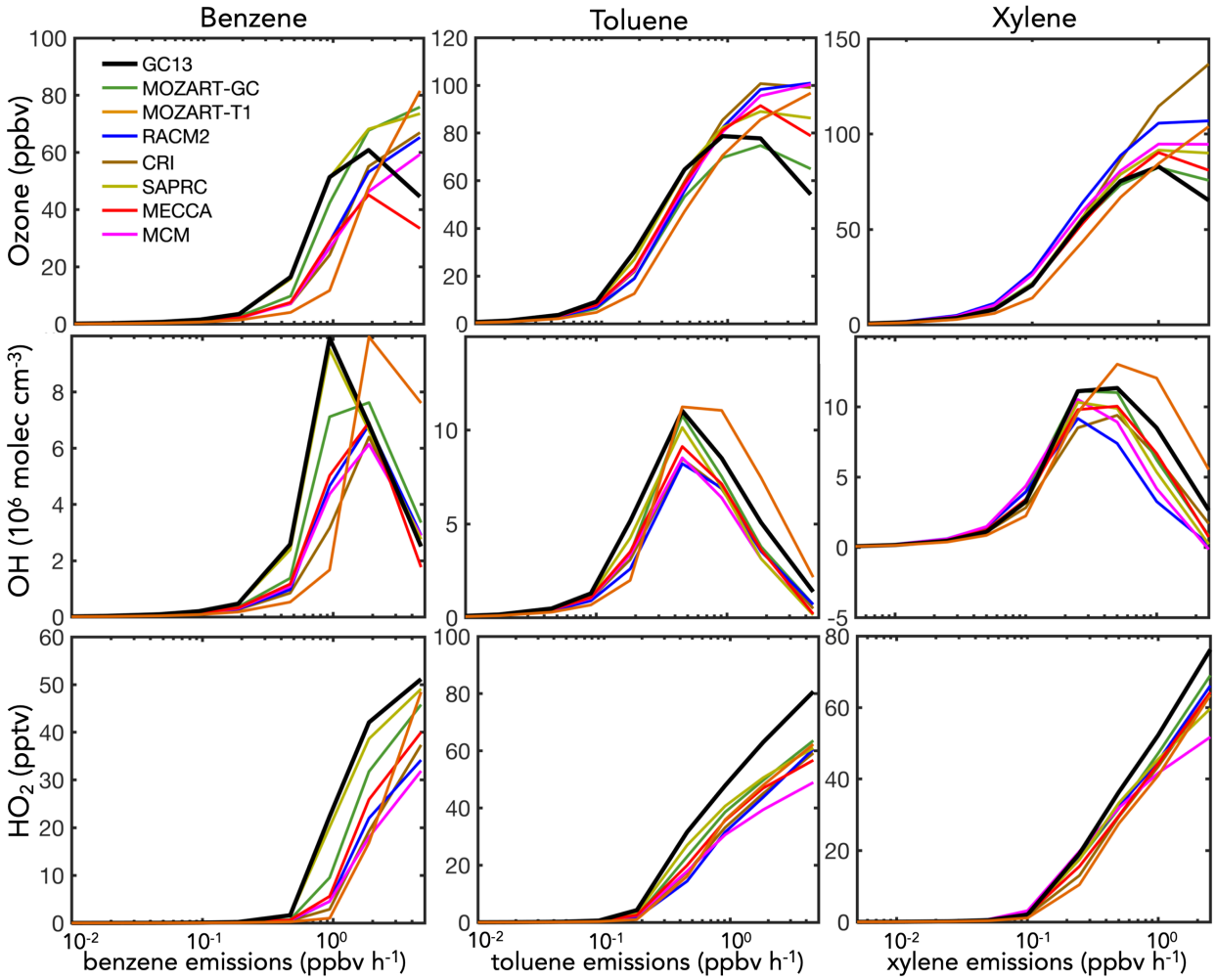

Figure S24. Like Figure S23, but at a higher fixed NO emission rate of 1 ppb h^{-1}, corresponding to a midday NO_x mixing ratio of ~7 ppb. Changes in OH, HO_2, and ozone concentrations are calculated by subtracting their midday (10:00-14:00) mean values in a simulation without aromatic emissions from those in an equivalent simulation with aromatic emissions.

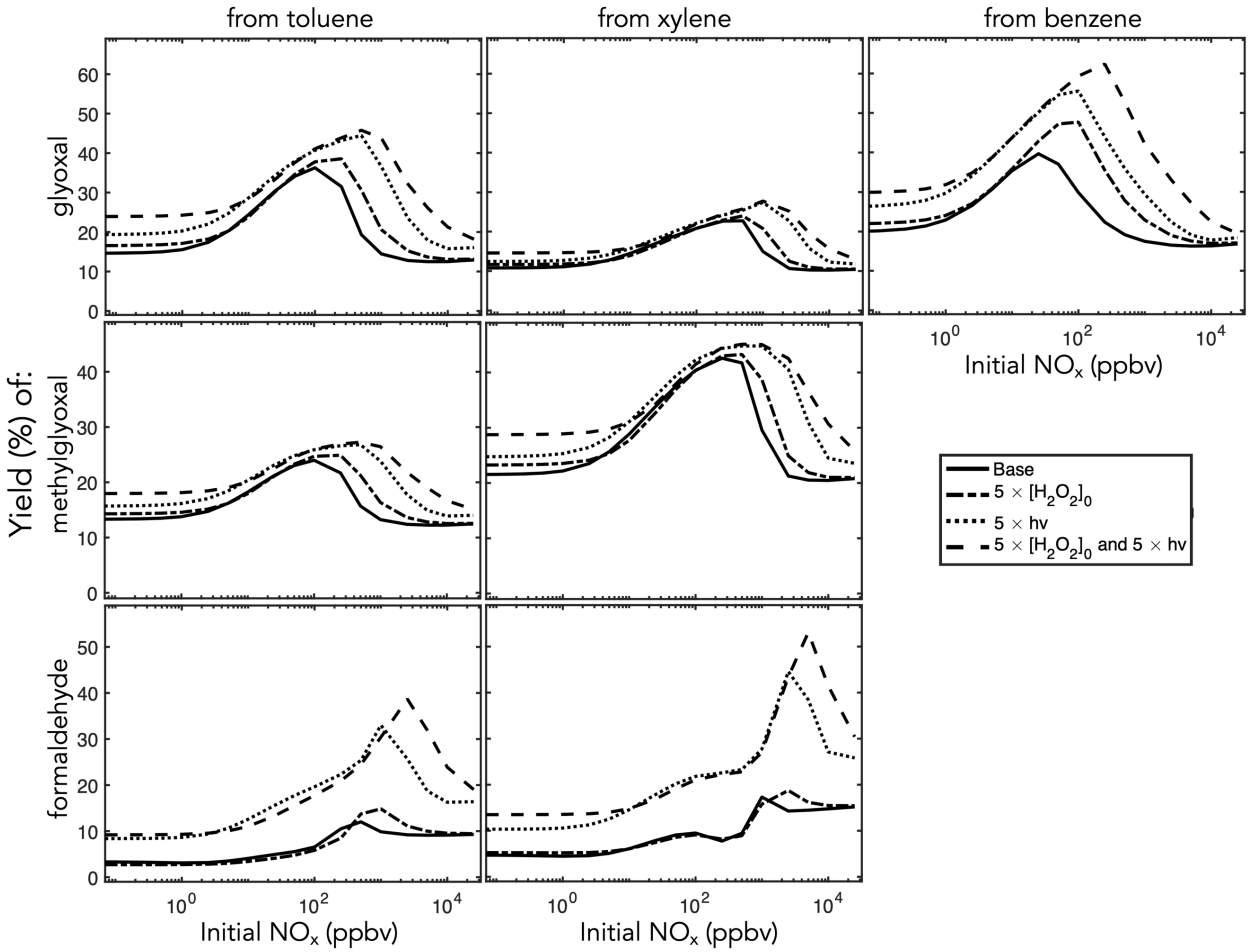

Figure S25. Sensitivity of initial (20 min) chamber yields to initial $[H_2O_2]$ and light flux. The base case has the same model setup as in Figures 4-6 of the main text. Light flux is increased by scaling all photolysis rates equally up by a factor of five.

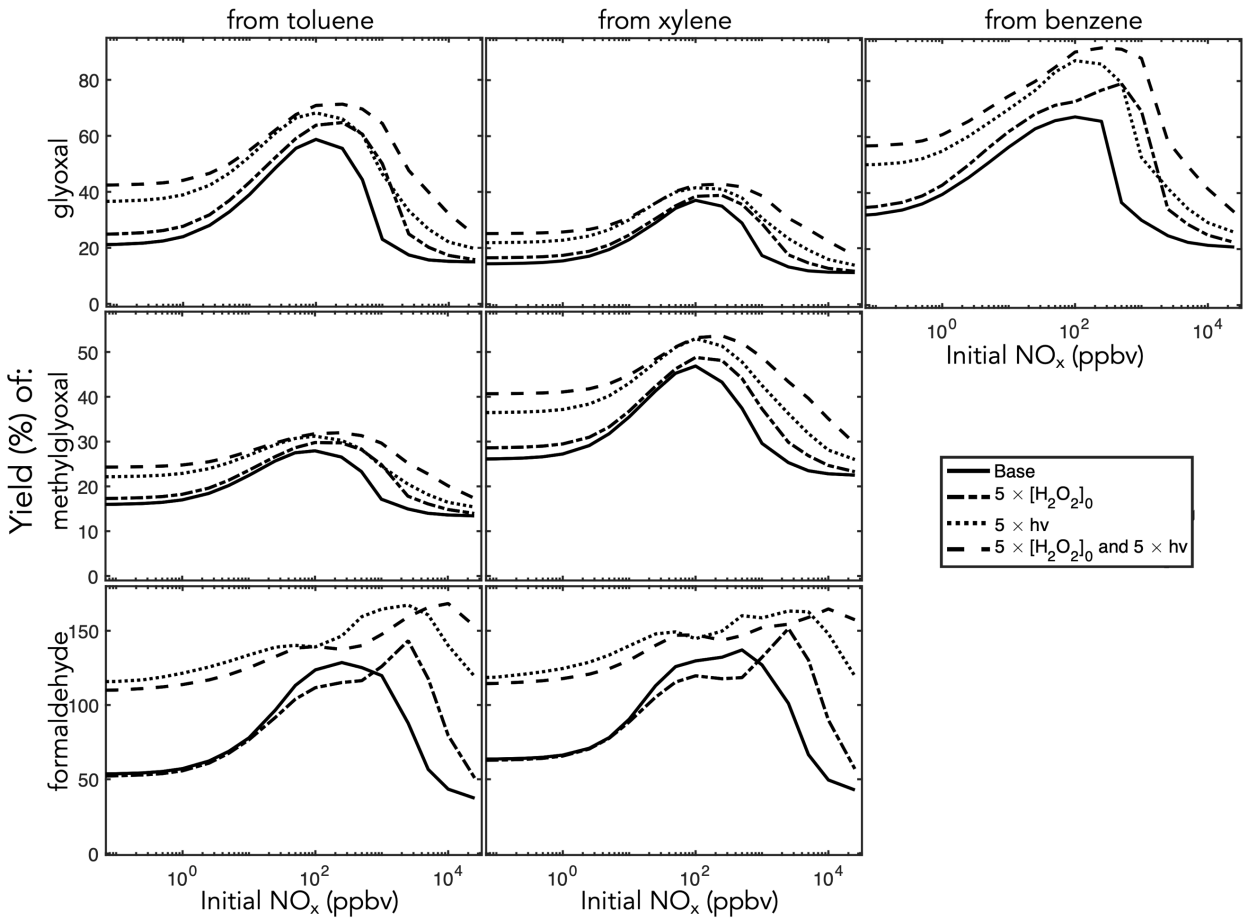

Figure S26. Sensitivity of long-term (24 h) chamber yields to initial $[H_2O_2]$ and light flux. The base case has the same model setup as in Figures S3-S5. Light flux is increased by scaling all photolysis rates equally up by a factor of five.

S5. Additional and precursor-specific mechanism perturbations in ambient simulations

Figure S27 is analogous to Figure 10 in the main text, but shows the individual effects of mechanism perturbations for each aromatic precursor, rather than the mixed emissions. Results are generally similar for each precursor, but tend to be stronger for benzene due to its higher initial yield of phenol relative to yields of ring-retaining products from toluene and xylene.

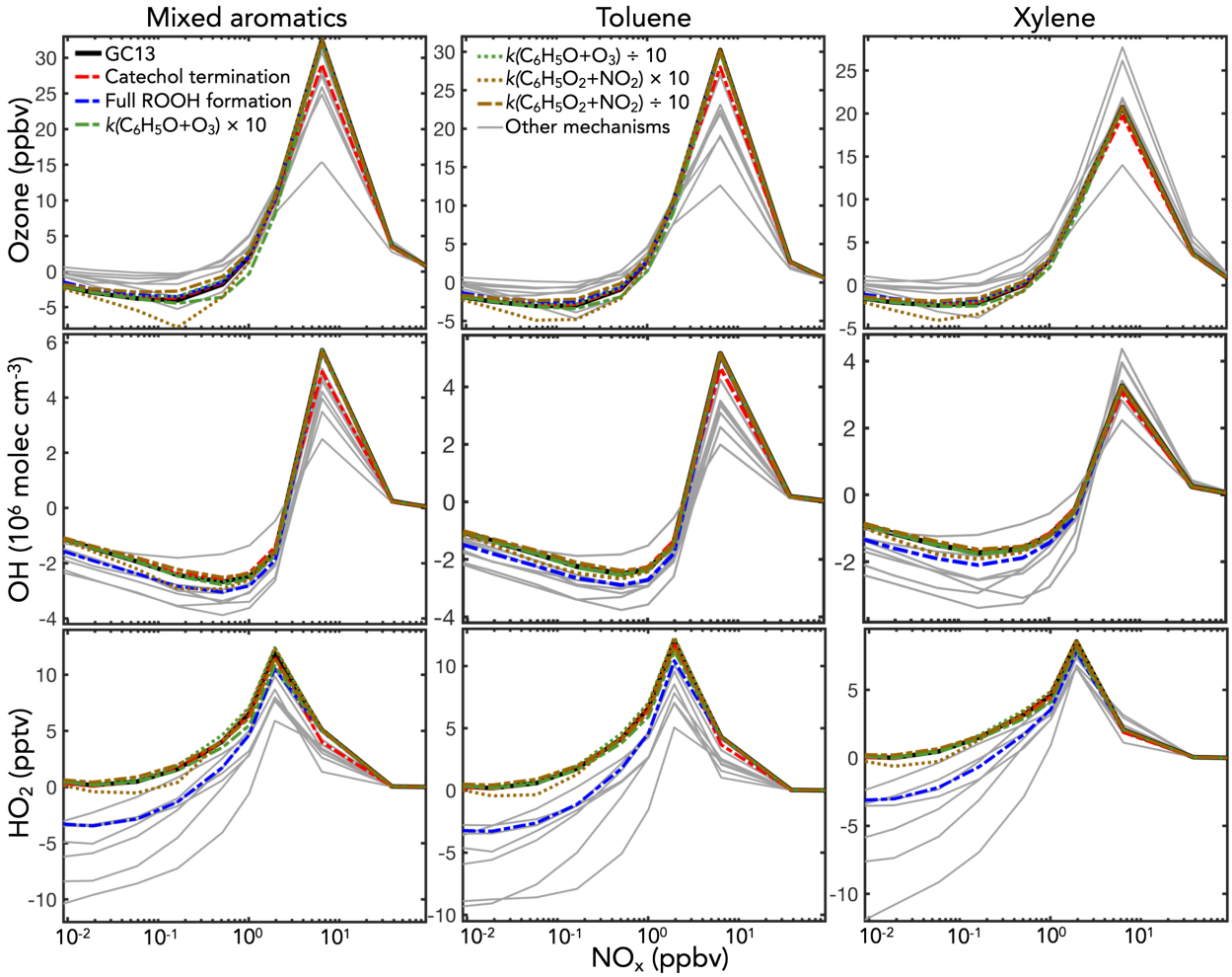

Figure S27: Changes in ozone, OH, and HO_2 due to perturbations in the aromatic oxidation mechanism in box model simulations of the continental boundary layer. GC13 is shown in black, other mechanisms are shown in gray, and specific perturbations to the GC13 mechanism (described in the text) are shown in colored and patterned lines. Changes in species concentrations are calculated by subtracting their midday (10:00-14:00) mean values in a simulation without aromatic emissions from those in an equivalent simulation with aromatic emissions, and are plotted against midday NO_x mixing ratio. Model setup is described in Section 4.1; the simulations plotted here have higher BTX emissions than in Figures 7-9 (x2) to better show perturbation sensitivities.

Figures S28-31 show the effects of additional perturbations. In Figures S28-S29, the red traces show that organonitrate formation (*i.e.* the addition of a 10% branching ratio from the initial aromatic peroxy radical reaction with NO to a radical-terminating, organonitrate product channel) has little impact on ozone or HO_x dynamics. The blue traces show a similarly small impact from removing any radical recycling from the benzoylperoxy radical + HO_2 reaction, and instead forming perbenzoic acid in 100% yield. The green traces show that modifications to the $C_6H_5O + NO_2$ rate have a similar impact to changes in the $C_6H_5O + O_3$ reaction (since the two are in direct competition), while the brown traces show that the $C_6H_5O_2 + NO_3$ reaction causes increased ozone titration at low-to-moderate NO_x.

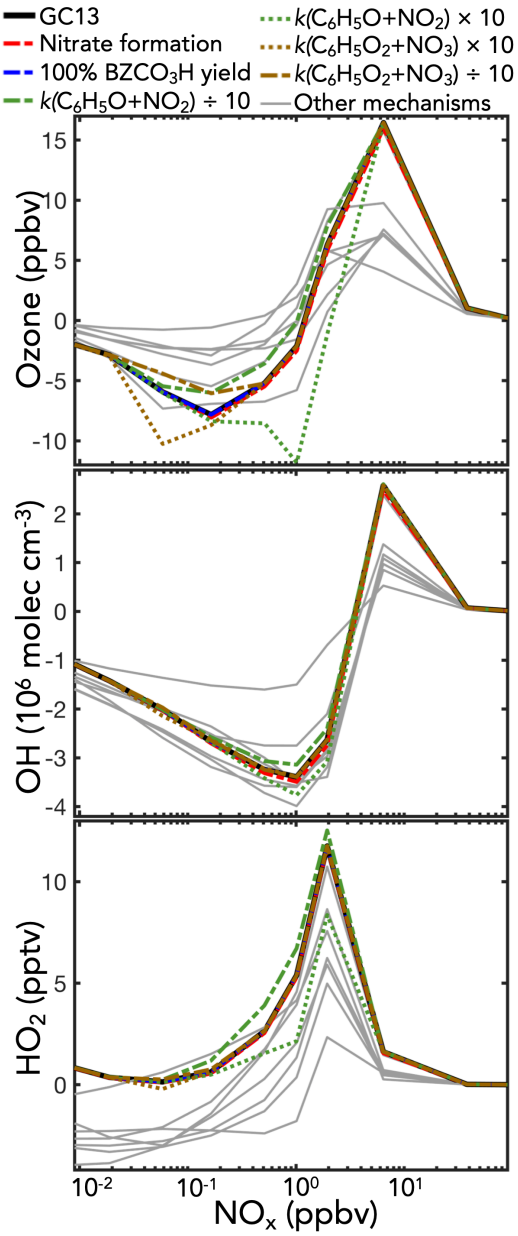

Figure S28. Changes in ozone, OH, and HO_2 due to perturbations in the aromatic oxidation mechanism in box model simulations of the continental boundary layer. Like Figure 10 in the main text, but with the colored traces showing a different set of perturbations, described above.

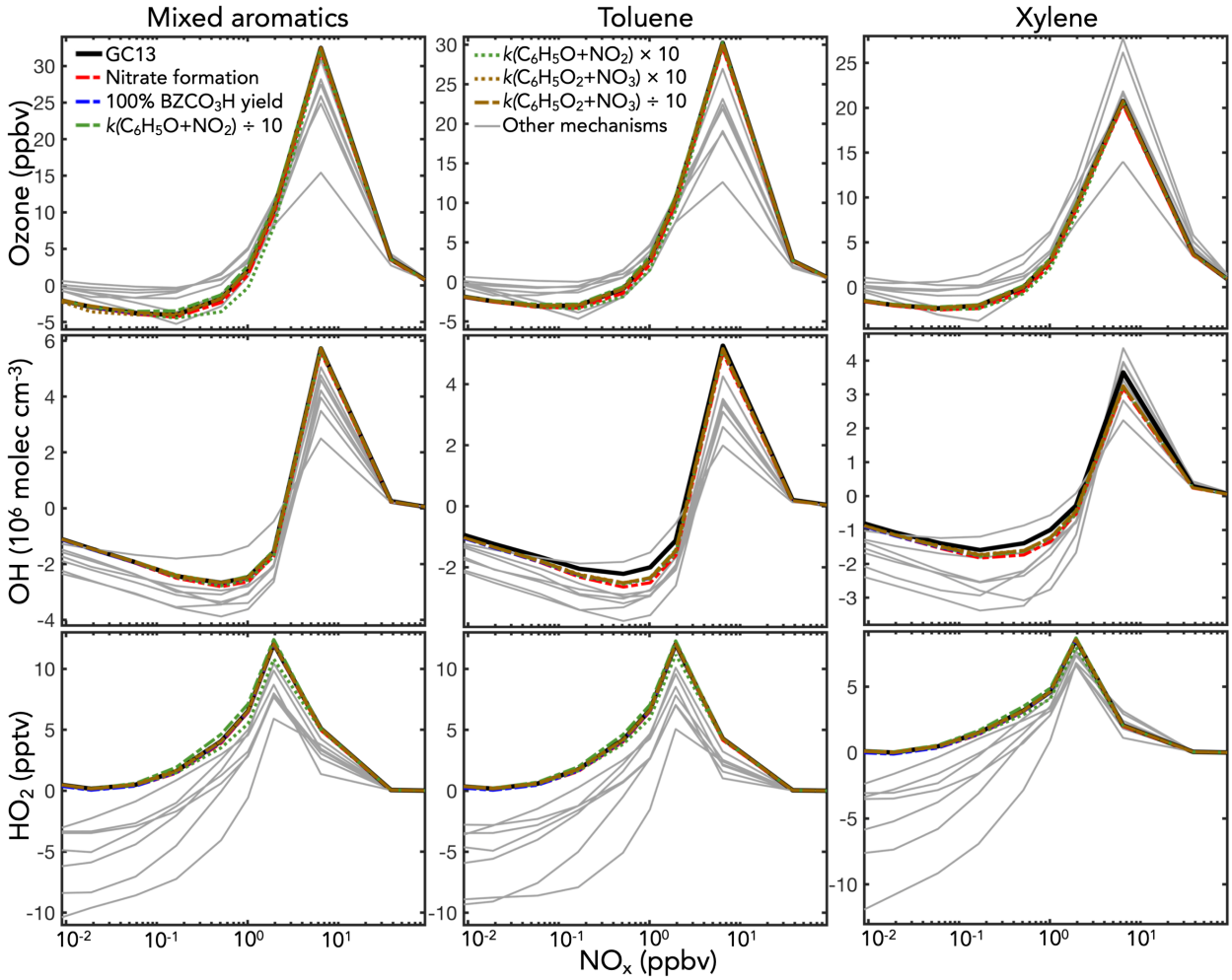

Figure S29. Like figure S28, but with individual simulations for each aromatic precursor.

Figures S30-S31 show the effects of perturbations to the rates of various nitrophenol loss processes. Taraborrelli *et al.*[17] recently described the importance of nitrophenol photolysis as a new pathway in MECCA, the only other mechanism analyzed here that includes this reaction, particularly for the formation of HONO.[13] Here, we find that, of the nitrophenol reactions, ozone is most sensitive to the photolysis rate, but overall the mechanism is largely insensitive to this minor chemical channel.

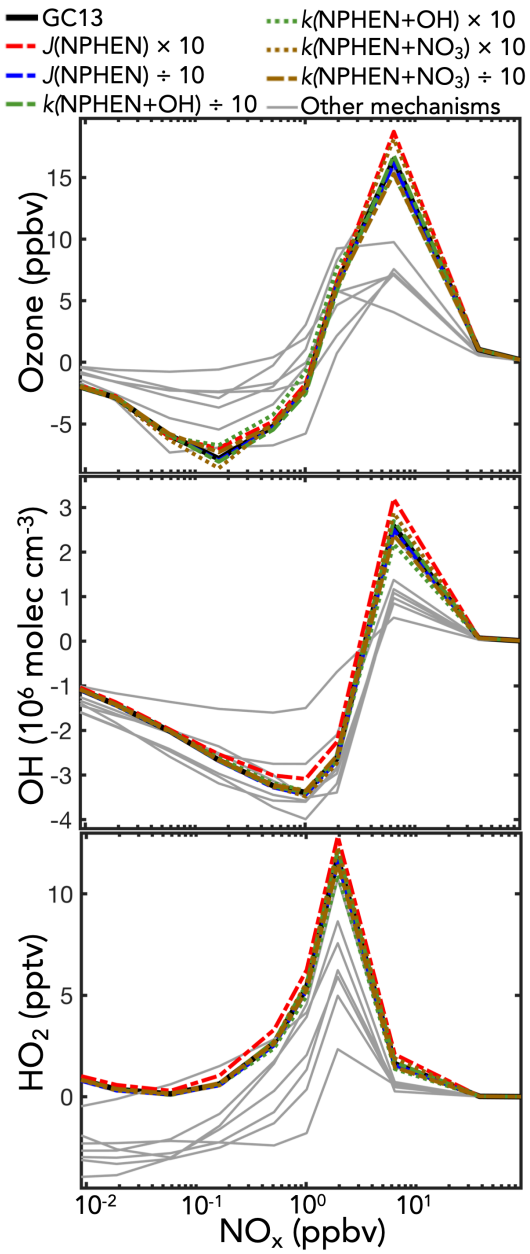

Figure S30. Changes in ozone, OH, and HO_2 due to perturbations in the aromatic oxidation mechanism in box model simulations of the continental boundary layer. Like Figure 10 in the main text, but with the colored traces showing a different set of perturbations, described above.

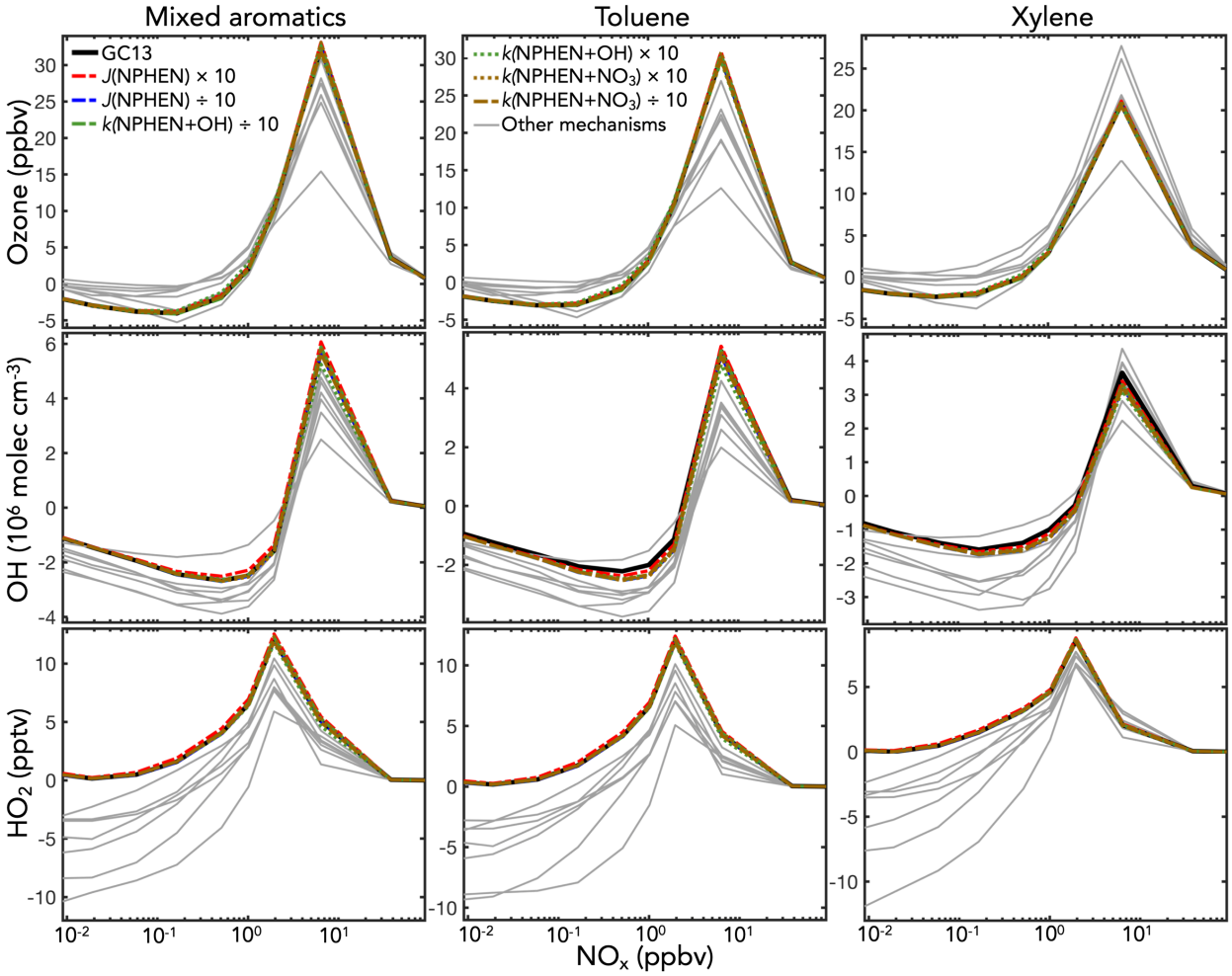

Figure S31. Like figure S30, but with individual simulations for each aromatic precursor.

S6. Diurnal NO_2, NO_3, and ozone patterns in ambient simulations

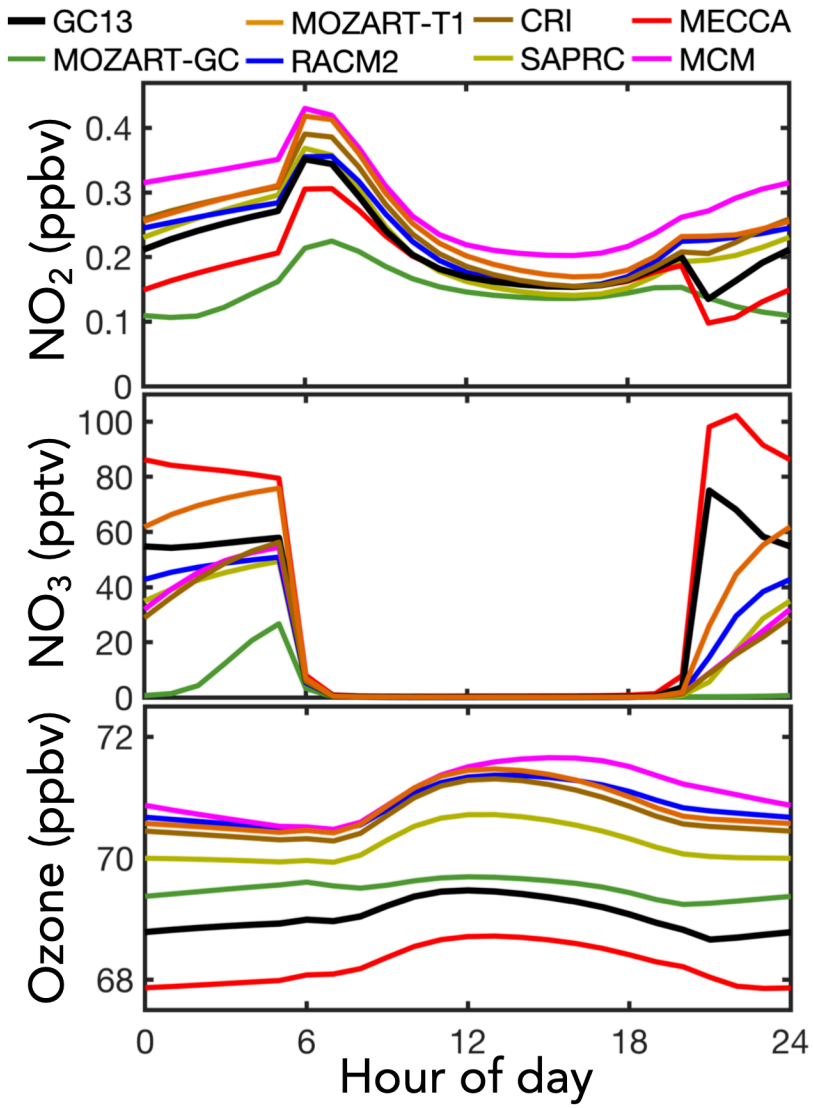

Figure S32. Diurnal patterns of NO_2, NO_3, and ozone concentrations in box model simulations of the continental boundary layer with different aromatic oxidation mechanisms. Model setup is described in Section 4.1. Simulations shown here have NO and BTX emissions of 40 and 120 ppt h^{-1} respectively, corresponding to midday mixing ratios of 0.2 and 1.5 ppb.

S7. Comparisons of GC13 to previous GEOS-Chem mechanisms in global simulations

In addition to the global simulations with the GC13, MOZART, and RACM mechanisms, we performed global simulations using three alternate mechanisms: MOZART-GC, GC12, and GC12r. MOZART-GC, as described in the main text, is the implementation of a reduced aromatic scheme derived from a previous MOZART version into GEOS-Chem. While its effects were described in detail by Porter *et al.,*[18] it was never incorporated into the standard GEOS-Chem code. As shown in Figures S33-S34, MOZART-GC exhibited low glyoxal and slightly low methylglyoxal relative to GC13, but overestimated ozone and OH concentrations in the Northern Hemisphere.

GC12 is the standard GEOS-Chem version 12 aromatic chemistry (also used in previous versions). It does not seek to treat aromatic chemistry explicitly; rather, it attempts to provide realistic yields of formaldehyde, glyoxal, and methylglyoxal from aromatic precursors as simply as possible:[19-20]

Benzene + OH → ARO_2 + 1.92 formaldehyde + 0.252 glyoxal + OH : $k = 2.33 \times 10^{-12} \times e^{(-193/T)}$
Toluene + OH → ARO_2 + 1.92 formaldehyde + 0.26 glyoxal + 0.215 methylglyoxal + OH : $k = 1.81 \times 10^{-12} \times e^{(338/T)}$
Xylene + OH → ARO_2 + 1.92 formaldehyde + 0.268 glyoxal + 0.463methylglyoxal + OH : $k = 2.31 \times 10^{-11}$
Xylene + NO_3 → no products : $k = 2.6 \times 10^{-16}$
ARO_2 + HO_2 → no products : $k = 1.4 \times 10^{-12} \times e^{(700/T)}$ *
ARO_2 + NO → no products : $k = 2.6 \times 10^{-12} \times e^{(350/T)}$ *

*(In practice, the RO_2 + HO_2/NO reactions are separated out between the benzene-, toluene-, and xylene-derived RO_2 radicals for diagnostic purposes).

This rudimentary mechanism has a number of shortcomings. First, it is not carbon-conserving, resulting in substantial loss of volatile organic mass. This prevents glyoxal and methylglyoxal formation in oxidative generations beyond the initial reaction with OH, resulting in lower concentrations of both in GC12 relative to GC13 (Figure S33). Second, the reactions of the aromatic peroxy radicals (ARO_2) with HO_2 and NO are completely radical-terminating, while in GC13 both are completely radical-propagating. As a result, GC12 exhibits lower ozone and HO_x radical concentrations than GC13 in regions with high aromatic emissions (Figure S34). As a rudimentary test of the significance of these shortcomings, we also simulate global chemistry with a revised GC12 mechanism, dubbed GC12r, in which the two ARO_2 reactions are changed as follow:

ARO_2 + HO_2 → generic C_{4+} hydroperoxide : $k = 1.4 \times 10^{-12} \times e^{(700/T)}$
ARO_2 + NO → NO_2 + generic C_{4+} aldehyde : $k = 2.6 \times 10^{-12} \times e^{(350/T)}$

The resulting mechanism remains highly simplified, but does exhibit ozone and OH concentrations more comparable to GC13 than GC12 (Figure S34). However, glyoxal and methylglyoxal remain excessively low (and entirely NO_x-independent), and the revised GC12-rmechanism now overestimates OH relative to GC13, possibly due to the 100% OH recycling in

the initial aromatic + OH reactions. GC-12r also simulates higher ozone and PAN but lower NO_3 than GC13, due to its lack of phenoxy-phenylperoxy radical dynamics. Furthermore, both GC12 and GC12r overestimate formaldehyde from aromatics, due largely to the implausible 192% yield from benzene.

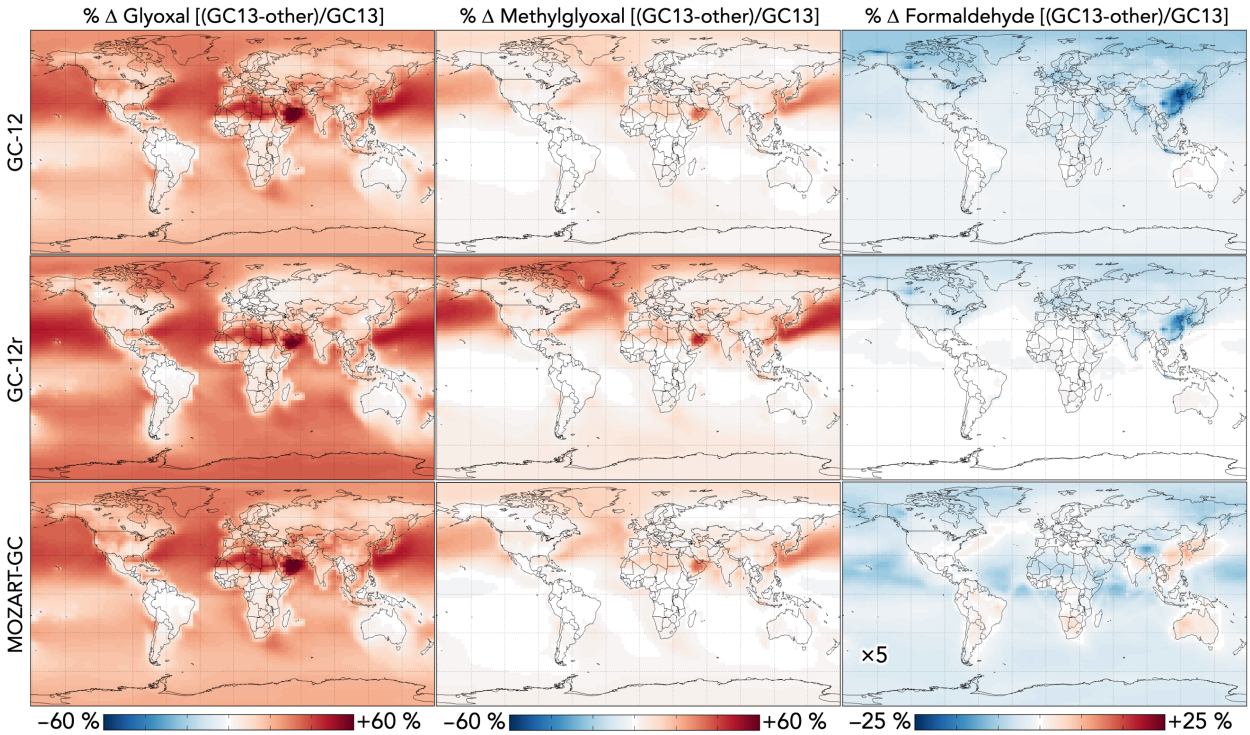

Figure S33. Differences in glyoxal, methylglyoxal, and formaldehyde concentrations between the GC13 mechanism and previously implemented GEOS-Chem mechanisms. Values are percent differences between the GC13 mechanism and the previous mechanism for annual mean concentrations in the bottom 1 km of the atmosphere, as simulated in GEOS-Chem (Section 5.1 of the main text). Formaldehyde differences in MOZART-GC are small relative to GC-12 and GC-12r; difference values are multiplied by a factored of five (i.e., they only span -5% to +5%).

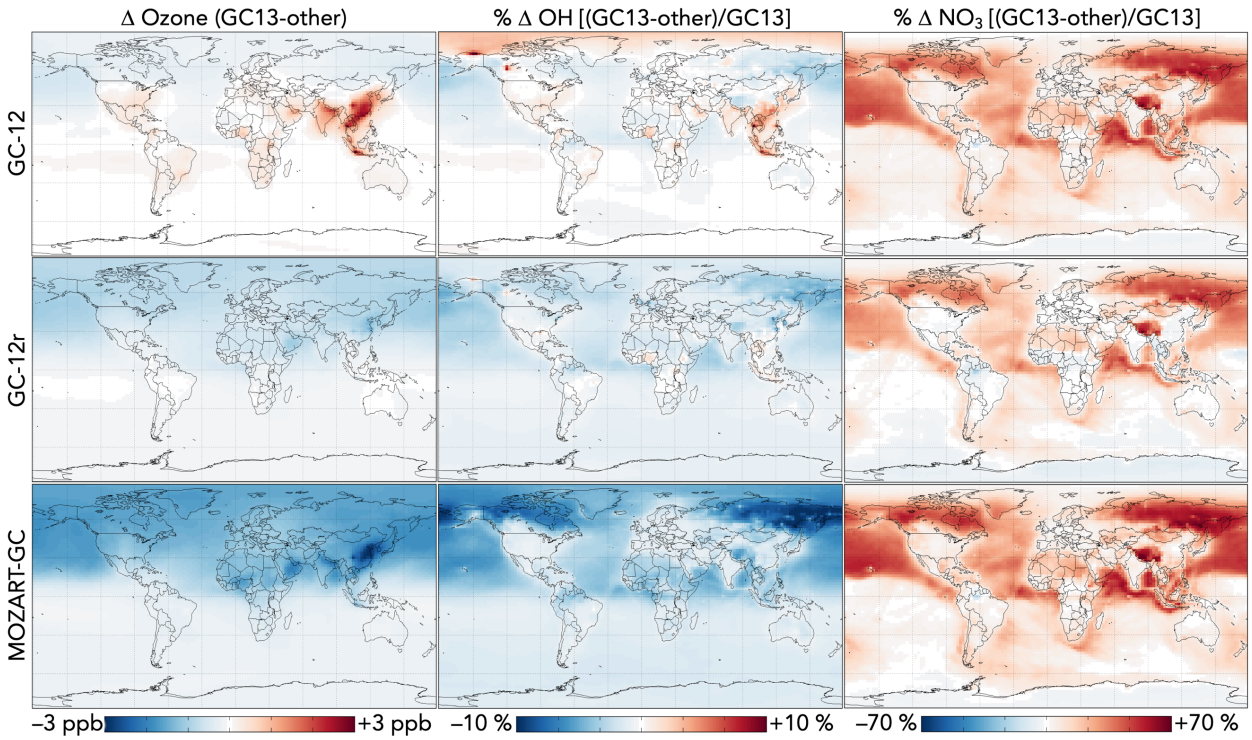

Figure S34. Differences in ozone, OH, and NO_3 concentrations between the GC13 mechanism and previously implemented GEOS-Chem mechanisms. Values are absolute (for ozone) and percent (for other species) differences between the GC13 mechanism and the previous mechanism for annual mean concentrations in the bottom 1 km of the atmosphere, as simulated in GEOS-Chem (Section 5.1 of the main text).

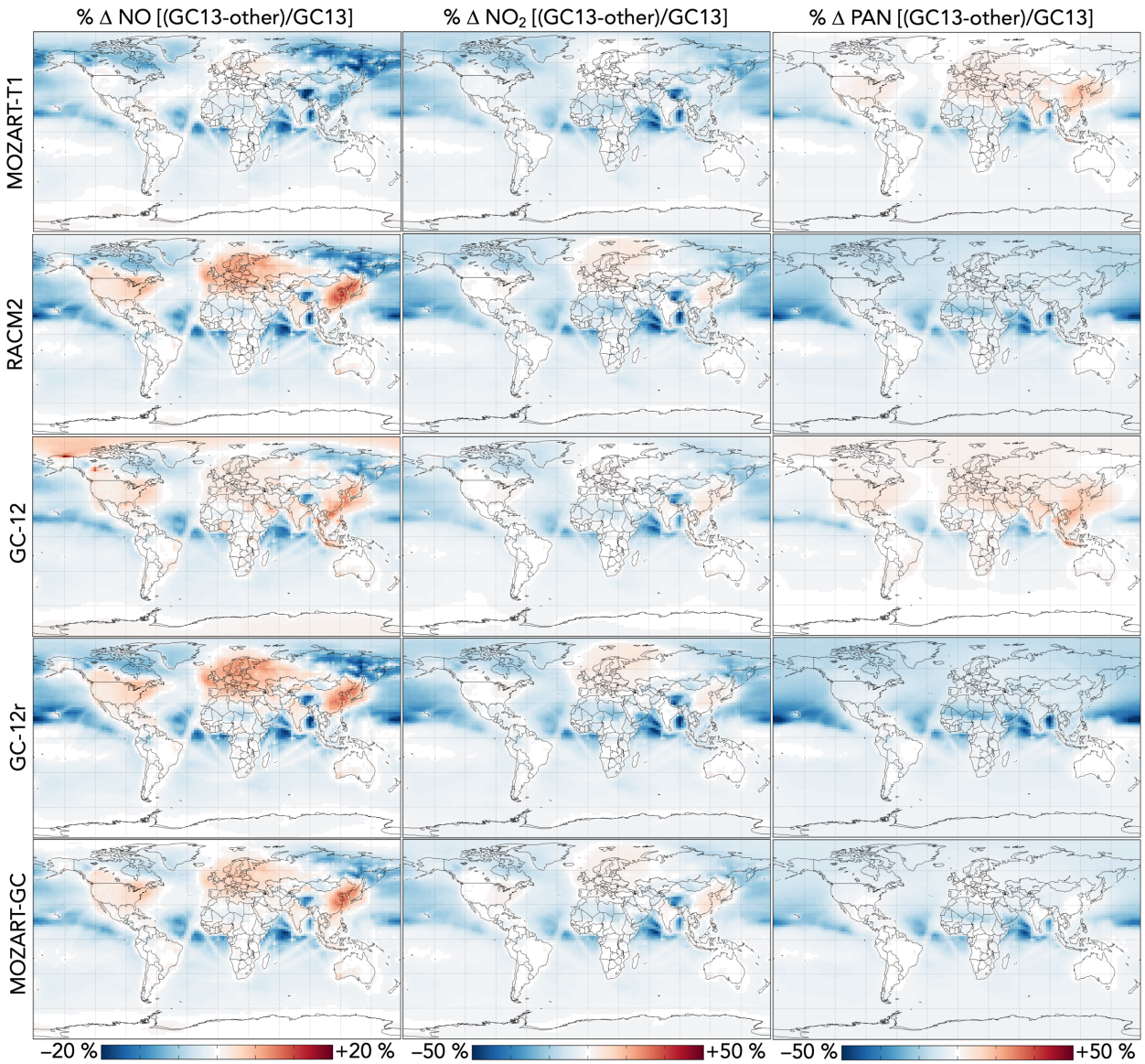

Figure S35. Differences in surface NO, NO_2, and PAN between the GC13 mechanism and MOZART, RACM, and previously implemented GEOS-Chem mechanisms. Values are percent differences between the GC13 mechanism and the other mechanism for annual mean concentrations in the bottom 1 km of the atmosphere, as simulated in GEOS-Chem (Section 5.1 of the main text).

S8. Global and regional output from GEOS-Chem modeling

Here we provide results from global simulations in greater detail. Figure S36 shows annual emissions of benzene, toluene, and xylene in GEOS-Chem with the emissions inventories described in the main text, as well as where those emitted VOCs are oxidized. Tables S5-S11 provide global and regional production, loss, and loading, and mean concentration values for species of interest in global simulations with each different mechanism, as well as a simulation with no aromatic chemistry, on both annual and seasonal means. Regions, selected primarily as hotspots of aromatic emissions, are defined in Table S12.

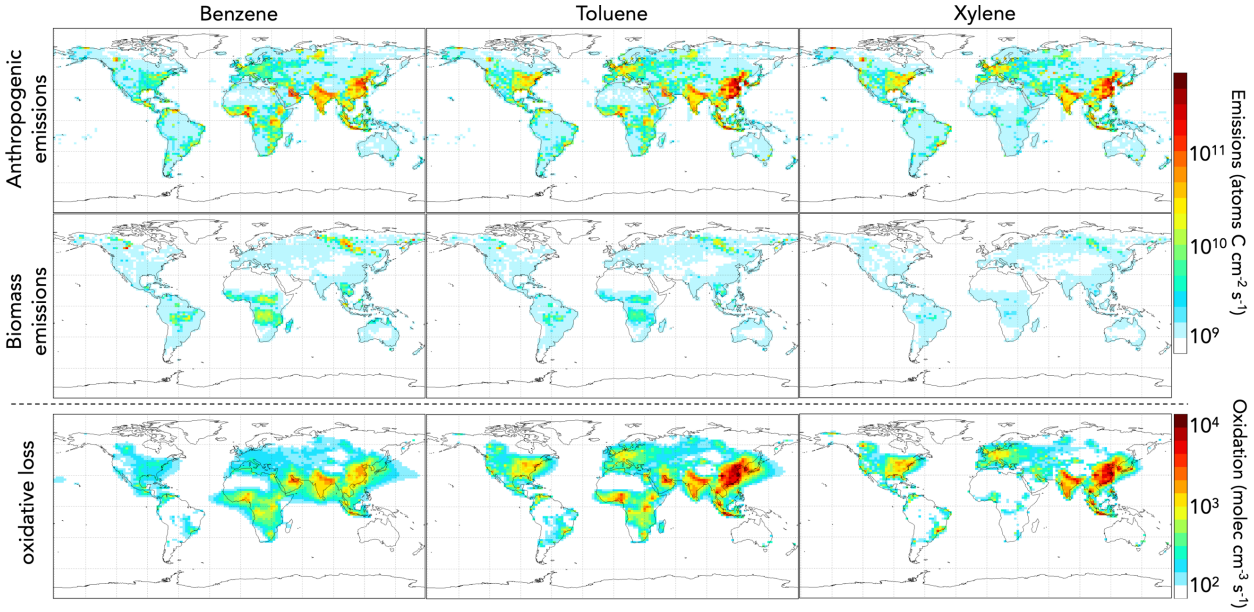

Figure S36. Annual anthropogenic emissions (top), biomass burning emissions (middle), and boundary layer oxidation (bottom) of benzene, toluene, and xylene in GEOS-Chem, with the model setup and emission inventory specifications described in Section 5.1 of the main text.

Table S5. Annual tropospheric production or loss (Tg y^{-1}) of key species in each mechanism[a]

Species	GC13	no aromatics	RACM2	MOZART	MOZART-GC	GC12	GC12r
Phenol	5.73	0	5.61	5.61	5.62	0	0
Cresols[b]	3.67	0	1.37	3.54	5.23	0	0
Catechols[c]	7.07	0	5.08	0	0	0	0
Benzaldehyde[d]	1.23	0	2.01	1.26	0	0	0
Nitrophenols	5.06	0	0	0	0	0	0
Ring-opened epoxides	0	0	12.21	5.31	1.70	0	0
Glyoxal	43.2	33.2	37.1	39.4	38.4	37.7	37.8
Methylglyoxal	148.8	142.0	147.0	146.2	144.0	145.6	146.2
Formaldehyde	1655	1672	1674	1670	1666	1661	1698
Acetic acid	45.4	43.2	44.5	43.5	44.7	43.6	44.3
Formic acid	43.0	39.5	39.4	39.6	39.4	39.3	39.5
CO	1694	1693	1706	1697	1692	1687	1722
Methane loss	591	604	600	602	596	590	604

[a]values show annual gas-phase production by all pathways except for the final line, which shows methane loss to reaction with OH; [b]including dimethylphenols; [c]including methyl and dimethylcatechols; [d]including tolualdehyde

Table S6. Annual regional production (Tg y^{-1}) of key species in each mechanism[a]

Region	Species	GC13	no aromatics	RACM2	MOZART	MOZART-GC	GC12	GC12r
NE China	Glyoxal	0.53	0.15	0.36	0.40	0.55	0.36	0.36
	Methylglyoxal	0.81	0.38	0.76	0.63	0.64	0.68	0.68
	Formaldehyde	4.25	3.96	4.29	4.05	4.26	4.89	5.10
	Acetic acid	0.150	0.076	0.089	0.080	0.086	0.081	0.089
	Formic acid	0.38	0.22	0.24	0.23	0.24	0.23	0.24
East China	Glyoxal	1.51	0.52	1.05	1.17	1.46	1.05	1.06
	Methylglyoxal	2.63	1.56	2.48	2.20	2.17	2.29	2.32
	Formaldehyde	13.80	13.29	13.86	13.39	13.80	15.23	15.96
	Acetic acid	0.48	0.29	0.33	0.30	0.32	0.30	0.33
	Formic acid	1.09	0.69	0.70	0.70	0.70	0.69	0.71
India	Glyoxal	1.13	0.70	0.91	0.96	1.03	0.91	0.91
	Methylglyoxal	2.13	1.74	2.05	1.96	1.94	1.99	2.01
	Formaldehyde	14.56	14.46	14.70	14.46	14.66	15.03	15.58
	Acetic acid	0.38	0.30	0.33	0.31	0.33	0.31	0.33
	Formic acid	0.90	0.74	0.74	0.74	0.74	0.73	0.75
Middle East	Glyoxal	0.184	0.041	0.099	0.124	0.124	0.096	0.097
	Methylglyoxal	0.193	0.115	0.175	0.158	0.143	0.155	0.156
	Formaldehyde	2.35	2.33	2.35	2.32	2.37	2.47	2.60
	Acetic acid	0.065	0.048	0.053	0.049	0.055	0.050	0.055
	Formic acid	0.091	0.041	0.041	0.041	0.041	0.040	0.041
Eq. Africa	Glyoxal	0.67	0.53	0.58	0.62	0.59	0.59	0.60
	Methylglyoxal	2.06	2.01	2.06	2.05	2.00	2.02	2.06
	Formaldehyde	8.42	8.55	8.53	8.53	8.46	8.55	8.84
	Acetic acid	0.38	0.36	0.37	0.36	0.38	0.36	0.37
	Formic acid	0.57	0.53	0.53	0.53	0.52	0.52	0.53
SE Asia	Glyoxal	0.43	0.29	0.36	0.39	0.40	0.36	0.37
	Methylglyoxal	1.01	0.85	0.98	0.95	0.92	0.95	0.97
	Formaldehyde	4.74	4.73	4.75	4.72	4.75	4.84	5.12
	Acetic acid	0.16	0.13	0.14	0.13	0.14	0.13	0.14
	Formic acid	0.35	0.30	0.29	0.30	0.29	0.28	0.29
NE USA	Glyoxal	0.164	0.097	0.135	0.141	0.164	0.136	0.136
	Methylglyoxal	0.45	0.37	0.44	0.42	0.42	0.43	0.43
	Formaldehyde	2.15	2.12	2.16	2.12	2.16	2.26	2.31
	Acetic acid	0.055	0.041	0.044	0.042	0.044	0.042	0.044
	Formic acid	0.138	0.112	0.112	0.112	0.112	0.111	0.112
N Europe	Glyoxal	0.127	0.067	0.106	0.110	0.138	0.105	0.106
	Methylglyoxal	0.33	0.26	0.33	0.30	0.31	0.31	0.32
	Formaldehyde	2.51	2.45	2.52	2.47	2.52	5.62	2.67
	Acetic acid	0.034	0.023	0.024	0.023	0.024	0.024	0.024
	Formic acid	0.109	0.085	0.086	0.085	0.086	0.086	0.086

[a]regions are defined in Table S11, and values are for the boundary layer within each region

Table S7. Annual mean tropospheric loading (Gg[a]) of key species in each mechanism

Species	GC13	no aromatics	RACM2	MOZART	MOZART-GC	GC12	GC12r
Glyoxal	17.16	13.51	14.95	15.39	15.02	14.88	14.87
Methylglyoxal	43.97	41.84	43.49	43.10	42.73	43.08	43.16
Formaldehyde	953.3	956.0	960.7	956.7	957.1	958.2	975.0
Acetic acid	390.5	363.1	378.1	366.8	381.6	373.3	374.6
Formic acid	631.6	577.7	580.6	581.2	581.6	583.9	578.8
Peroxyacyl nitrate	1965	1935	2051	1960	2022	1915	2057
CO (Tg)	316.3	306.2	311.2	308.4	311.5	314.5	310.4
Ozone (Tg)	325.8	328.3	329.2	328.7	327.7	324.5	330.3

[a]unless otherwise noted

Table S8. Annual mean tropospheric concentrations of key species in each mechanism

Species	GC13	no aromatics	RACM2	MOZART	MOZART-GC	GC12	GC12r
CO (ppb)	72.33	69.99	71.15	70.53	71.21	71.93	70.96
Ozone (ppb)	72.19	72.56	72.70	72.62	72.50	71.89	72.90
OH (10^6 molec cm^{-3})	1.222	1.250	1.239	1.244	1.235	1.220	1.247
HO_2 (ppt)	4.848	4.815	4.846	4.826	4.836	4.848	4.842
NO (ppt)	27.92	28.48	28.02	28.32	28.12	27.35	28.17
NO_2 (ppt)	55.82	57.99	56.98	57.64	56.83	55.67	57.26
NO_3 (ppt)	1.056	0.866	0.851	0.866	0.805	0.830	0.878
HONO (ppt)	0.445	0.462	0.448	0.456	0.450	0.438	0.452

Table S9. Annual mean global surface concentrations (ppt[a]) of key species in each mechanism

Species	GC13	no aromatics	RACM2	MOZART	MOZART-GC	GC12	GC12r
Glyoxal	7.5	6.2	6.8	6.9	6.9	6.7	6.7
Methylglyoxal	15.4	14.6	15.3	15.1	15	15.1	15.2
Formaldehyde	473.9	473.1	477.2	474	475.4	479.2	487.3
Acetic acid	61.9	57.7	59.6	58.1	59.9	58.5	59.3
Formic acid	124.7	114.6	114.7	114.9	114.6	114.5	114.6
Peroxyacyl nitrate	79.6	76.1	85.1	78.4	82.3	76.8	85.6
CO (ppb)	86.07	83.47	84.77	84.02	84.8	85.54	84.6
Ozone (ppb)	28.89	29.24	29.49	29.33	29.23	28.85	29.63
OH (10^6 molec cm^{-3})	1.084	1.109	1.102	1.105	1.097	1.085	1.109
HO_2	4.532	4.517	4.554	4.531	4.537	4.525	4.565
NO	17.7	18.6	17.1	18	17.3	17.2	17.5
NO_2	140.8	146.5	141	144.3	140.1	140.8	141.2
NO_3	2.66	2.46	2.43	2.46	2.3	2.35	2.49
HONO	1.23	1.29	1.21	1.26	1.21	1.21	1.21

[a]unless otherwise noted

Table S10. Percent difference in annual mean regional surface concentrations of key species when switching from a simulation with no aromatic oxidation to each individual mechanism

Region	Species	GC13	RACM2	MOZART	MOZART-GC	GC12	GC12r
NE China	Glyoxal	55.1	35.0	30.7	48.4	28.0	26.9
	Methylglyoxal	72.6	66.2	42.8	45.7	52.2	52.4
	Formaldehyde	8.8	9.9	3.1	8.0	24.4	29.9
	Acetic Acid	77.3	17.3	4.5	14.0	7.8	16.1
	Formic Acid	19.4	1.0	0.4	0.9	0.5	1.0
	Peroxyacyl nitrate	30.1	41.3	12.2	31.1	15.9	40.9
	CO	2.2	1.7	0.6	1.1	2.0	1.8
	Ozone	5.5	10.4	3.9	7.7	2.7	10.6
	OH	0.5	0.5	-0.1	3.3	0.5	2.1
	HO_2	14.2	16.6	6.2	14.7	13.0	17.0
	NO	-17.6	-26.5	-11.4	-25.0	-19.0	-24.7
	NO_2	-8.3	-11.9	-4.5	-12.2	-10.5	-11.4
	NO_3	0.4	1.4	1.6	-2.8	-2.9	2.4
	HONO	-7.5	-10.8	-4.0	-9.9	-10.4	-10.0
East China	Glyoxal	49.6	28.3	27.2	37.2	23.8	23.2
	Methylglyoxal	47.9	41.9	27.7	27.6	33.0	33.3
	Formaldehyde	6.0	6.7	1.8	5.3	16.9	21.9
	Acetic Acid	54.0	14.9	3.6	13.0	6.9	13.7
	Formic Acid	18.6	0.6	0.2	0.5	0.0	0.7
	Peroxyacyl nitrate	22.8	32.0	9.2	23.7	9.0	32.4
	CO	2.6	1.9	0.7	1.3	2.3	2.1
	Ozone	2.9	6.8	2.5	4.6	0.0	7.3
	OH	-3.1	-3.6	-1.5	-1.7	-4.6	-1.5
	HO_2	7.3	8.3	3.2	7.1	5.8	9.1
	NO	-15.9	-23.8	-10.2	-22.3	-18.0	-22.3
	NO_2	-8.6	-11.6	-4.6	-12.2	-10.9	-11.2
	NO_3	1.2	-0.1	0.9	-6.9	-5.9	1.9
	HONO	-9.7	-13.3	-5.2	-12.4	-12.9	-12.5
India	Glyoxal	31.9	18.4	16.1	20.5	13.7	13.1
	Methylglyoxal	16.9	13.2	8.6	8.4	10.9	10.8
	Formaldehyde	2.4	3.2	0.6	2.4	5.0	8.5
	Acetic Acid	27.6	11.0	2.2	10.8	5.2	9.9
	Formic Acid	8.7	0.3	0.2	0.3	0.2	0.3
	Peroxyacyl nitrate	8.1	14.2	3.0	10.1	-0.4	14.9
	CO	2.8	2.0	0.7	1.6	2.6	2.1
	Ozone	-0.1	2.1	0.7	0.9	-1.9	2.7
	OH	-3.7	-2.9	-1.2	-2.5	-4.4	-1.6
	HO_2	1.8	2.6	0.9	1.9	1.2	3.2
	NO	-3.3	-4.8	-1.5	-4.4	-4.6	-4.7
	NO_2	-2.8	-2.0	-0.8	-3.3	-3.1	-2.0
	NO_3	2.4	-1.8	0.0	-6.2	-5.3	0.1
	HONO	-4.0	-4.3	-1.6	-4.6	-5.9	-3.6

Table S10 cont'd

Region	Species	GC13	RACM2	MOZART	MOZART-GC	GC12	GC12r
Middle East	Glyoxal	273.6	116.0	127.6	131.3	85.7	85.9
	Methylglyoxal	55.2	41.6	28.1	19.4	27.9	27.7
	Formaldehyde	1.9	1.8	0.2	2.1	4.8	8.7
	Acetic Acid	25.8	10.2	1.8	12.5	4.6	10.5
	Formic Acid	21.4	0.4	0.2	0.4	0.5	0.2
	Peroxyacyl nitrate	5.5	11.4	2.7	11.1	-3.1	14.4
	CO	4.3	2.5	1.0	2.3	3.5	2.7
	Ozone	-0.9	1.2	0.5	0.5	-2.1	2.0
	OH	-3.3	-3.4	-1.4	-2.9	-4.6	-1.7
	HO_2	3.6	2.8	1.5	2.8	1.9	4.2
	NO	-2.8	-3.7	-1.3	-3.9	-5.3	-3.9
	NO_2	-3.5	-1.6	-0.6	-3.6	-4.0	-1.5
	NO_3	1.6	-3.9	-0.1	-9.5	-5.3	-1.6
	HONO	-4.2	-4.4	-1.6	-4.8	-6.7	-3.6
N Eq. Africa	Glyoxal	22.0	7.8	11.5	6.7	7.1	8.2
	Methylglyoxal	3.1	2.5	2.0	0.8	1.3	2.0
	Formaldehyde	0.0	0.6	0.1	0.3	0.9	3.3
	Acetic Acid	7.0	3.8	0.8	5.7	2.1	3.6
	Formic Acid	6.9	-0.2	0.1	-0.5	-0.7	0.1
	Peroxyacyl nitrate	-4.4	1.1	0.3	-1.4	-6.3	3.3
	CO	2.3	1.3	0.5	1.3	1.9	1.2
	Ozone	-2.4	0.0	0.0	-1.3	-2.8	0.9
	OH	-4.7	-2.3	-1.1	-3.8	-4.5	-0.9
	HO_2	-0.4	0.3	0.2	-0.5	-0.9	1.1
	NO	-1.9	-1.6	-0.5	-2.5	-3.1	-1.4
	NO_2	-4.4	-0.7	-0.3	-3.9	-3.1	0.0
	NO_3	3.6	-4.1	-1.1	-14.7	-9.8	0.5
	HONO	-4.7	-1.9	-0.9	-4.7	-4.3	-0.8
SE Asia	Glyoxal	44.6	21.6	26.1	27.2	21.4	22.3
	Methylglyoxal	24.6	19.7	14.1	11.8	17.7	17.6
	Formaldehyde	2.4	2.9	0.6	2.6	4.9	9.1
	Acetic Acid	21.1	9.1	2.2	9.5	4.3	8.1
	Formic Acid	8.9	-0.8	0.0	-0.8	-1.8	-0.3
	Peroxyacyl nitrate	8.5	13.1	3.0	10.3	-6.1	14.4
	CO	2.5	1.7	0.7	1.4	2.3	1.8
	Ozone	-0.2	1.6	0.6	0.3	-4.7	2.5
	OH	-5.6	-6.4	-2.3	-5.6	-9.9	-3.8
	HO_2	2.4	2.4	1.1	2.1	0.2	3.3
	NO	-3.0	-4.3	-1.2	-4.3	-6.3	-3.6
	NO_2	-1.7	-0.8	-0.3	-4.0	-4.0	-0.3
	NO_3	0.4	-2.2	-0.3	-14.3	-13.8	2.3
	HONO	-5.2	-5.7	-2.3	-7.3	-10.0	-3.9

Table S10 cont'd

Region	Species	GC13	RACM2	MOZART	MOZART-GC	GC12	GC12r
	Glyoxal	56.6	31.9	32.0	49.0	29.1	29.0
	Methylglyoxal	20.6	19.3	12.4	13.4	15.8	15.9
	Formaldehyde	2.6	3.1	0.8	2.9	7.8	9.6
	Acetic Acid	20.9	6.2	1.2	6.1	2.9	5.3
	Formic Acid	10.8	0.0	0.0	0.0	-0.2	0.1
	Peroxyacyl nitrate	8.6	14.5	4.0	11.1	3.2	13.9
NE	CO	3.4	1.9	0.7	1.7	2.7	1.8
USA	Ozone	-0.3	2.5	0.9	1.3	-0.8	2.8
	OH	-0.8	-0.7	-0.3	0.7	-1.2	0.3
	HO_2	4.0	4.6	1.8	4.4	3.6	4.7
	NO	-4.2	-8.9	-3.2	-8.0	-6.9	-8.4
	NO_2	-3.2	-5.3	-1.9	-5.6	-5.0	-5.0
	NO_3	-0.7	-1.3	0.1	-5.6	-4.5	0.1
	HONO	-0.4	-2.0	-0.8	-0.7	-2.2	-1.8
	Glyoxal	42.0	26.2	25.0	40.4	22.2	22.0
	Methylglyoxal	27.2	29.0	18.5	20.9	23.1	23.6
	Formaldehyde	2.6	3.3	1.0	2.7	7.8	9.7
	Acetic Acid	30.6	6.9	1.4	6.4	3.1	6.0
	Formic Acid	13.6	0.3	0.1	0.3	0.2	0.3
	Peroxyacyl nitrate	9.3	15.2	4.2	10.7	4.1	15.0
N	CO	3.7	2.0	0.7	1.9	2.9	1.8
Europe	Ozone	-0.1	2.7	1.0	1.5	-0.2	3.0
	OH	0.4	1.3	0.4	2.3	1.0	1.7
	HO_2	4.0	5.0	1.9	4.5	3.9	5.1
	NO	-2.7	-8.8	-3.4	-6.8	-3.8	-8.8
	NO_2	-1.4	-3.6	-1.3	-3.1	-2.3	-3.7
	NO_3	0.8	0.5	0.5	-1.8	-1.7	1.3
	HONO	0.5	-0.4	-0.3	0.5	-0.5	-0.5

Table S11. Percent difference in seasonal mean regional surface concentrations of key species when switching from a simulation with no aromatic oxidation to each mechanism[a]

Region	Species	GC13	RACM2	MOZART	MOZART-GC	GC12	GC12r
NE China	OH	16.37,4.26, -3.60,3.17	22.24,4.81, -4.74,3.66	6.59,1.63, -1.83,1.05	27.85,8.39, -2.94,7.62	21.11,5.23, -4.92,4.27	23.29,6.59, -2.94,5.11
	Ozone	8.80,5.39, 2.65,7.79	18.85,10.43, 5.25,12.90	6.97,4.04, 1.82,4.84	15.79,7.80, 2.64,10.07	9.73,2.94, -1.62,4.47	17.54,10.87, 5.82,12.84
E China	OH	1.46,-2.45, -4.12,-3.08	1.46,-2.45, -4.12,-3.08	2.57,-2.67, -4.99,-3.73	0.30,-1.06, -1.91,-1.53	2.23,-3.62, -6.40,-4.68	4.92,-0.57, -3.06,-1.51
	Ozone	5.07,2.37, 1.18,3.86	5.07,2.37, 1.18,3.86	12.22,6.31, 3.25,7.74	9.49,4.30, 1.21,5.41	4.50,-0.20, -2.66,0.13	12.30,6.90, 3.86,8.15
India	OH	-4.82,-3.00 -3.32,-4.17	-2.32,-2.17, -3.13,-3.57	-1.25,-1.01, -1.16,-1.37	-2.39,-1.77, -2.52,-3.11	-4.25,-3.31, -4.64,-5.14	-0.39,-1.17, -2.08,-1.96
	Ozone	0.15,-0.43, -0.34,-0.11	3.44,1.32, 1.17,2.18	1.15,0.36, 0.34,0.66	1.54,0.61, 0.54,0.93	-1.24,-1.74, -2.38,-2.28	4.26,1.76, 1.64,2.81
Middle East	OH	-3.37,-3.73, -2.74,-3.62	-3.54,-3.51, -2.82,-3.83	-1.18,-1.40, -1.28,-1.66	-2.10,-3.06, -2.82,-3.33	-4.49,-5.00, -3.94,-5.02	-1.52,-1.78, -1.41,-1.96
	Ozone	-1.02,-1.27, 0.40,-0.81	2.34,0.98, 0.65,1.14	1.14,0.43, 0.19,0.42	1.17,0.33, 0.25,0.64	-1.81,-2.40, -1.68,-2.31	3.40,1.84, 1.18,1.99
N Eq. Africa	OH	-5.76,-4.05, -4.82,-4.79	-2.74,-2.11, -2.26,-2.38	-1.53,-1.00, -1.02,-1.06	-3.47,-3.52, -4.09,-4.30	-4.85,-4.09, -4.87,-4.90	-1.14,-0.79, -0.75,-0.85
	Ozone	-2.35,-2.26, -2.62,-2.78	0.50,-0.11, -0.15,-0.23	0.25,-0.08, -0.06,-0.08	-0.77,-1.36, -1.44,-1.76	-2.66,-2.66, -2.92,-3.29	1.42,0.71, 0.69,0.67
SE Asia	OH	-6.13,-5.11, -5.67,-5.92	-6.55,-5.90, -6.75,-6.82	-2.77,-2.09, -2.31,-2.39	-5.71,-5.09, -5.91,-6.22	-9.94,-8.71, -9.98,-11.33	-3.68,-3.59 -4.20,-3.91
	Ozone	-0.01,-0.43, -0.80,-0.06	2.03,1.17, 0.75,1.99	0.76,0.41, 0.32,0.68	0.43,0.06, -0.14,0.36	-4.95,-4.34, -4.20,-5.52	3.13,1.85, 1.30,2.93
NE USA	OH	12.30,-0.61, -2.67,-0.17	18.08,-0.27, -3.38,-0.09	5.39,-0.02, -1.19,-0.06	22.19,1.72, -2.85,1.59	15.11,-0.33, -4.07,-0.26	16.96,0.93, -2.08,0.54
	Ozone	-0.17,-1.04, -0.09,0.43	5.82,2.62, 0.74,2.33	2.12,1.03, 0.24,0.88	3.77,1.19, -0.06,1.40	1.08,-1.05, -1.76,-0.43	5.76,3.11, 1.02,2.45
N Europe	OH	3.25,1.56, -0.65,1.90	7.67,3.49, -0.57,2.99	2.12,1.18, -0.16,0.95	8.07,4.46, 0.34,4.07	4.64,2.86, -0.59,2.46	7.19,4.16, -0.11,3.15
	Ozone	-2.37,-0.33, 0.71,1.05	3.43,3.42, 1.42,3.16	1.25,1.27, 0.50,1.17	1.04,1.84, 0.86,2.09	-0.81,-0.01, -0.36,0.45	3.83,3.95, 1.59,3.30

[a]format is winter, spring, summer, fall

Table S12. Boundaries and annual aromatic oxidation (Tg y^{-1}) for regions referred to herein

Region	Latitude	Longitude	Benzene + OH	Toluene + OH	Xylene + OH
Northeast China	29-41 N	111.25-121.25 E	0.099	0.596	0.590
East China	21-43 N	103.75-123.75 E	0.268	1.560	1.478
India	7-33 N	73.75-91.25 E	0.284	0.444	0.590
Middle East	21-31 N	46.25-56.25 E	0.115	0.176	0.034
N Equatorial Africa	1 S-15 N	6.25 W – 11.25 E	0.109	0.229	0.043
Southeast Asia[a]	9-17 N	98.75-106.25 E	0.034	0.112	0.132
	5-9 N	106.25-113.75 E	0.034	0.099	0.130
Northeast US	39-45 N	68.75-88.75 W	0.014	0.099	0.130
Northern Europe	45-55 N	3.75 W – 21.25 E	0.017	0.088	0.125

[a]values are totaled/averaged across two distinct boxes, focused on emission hotspots in Thailand and Java.

S9. References

1. Cabrera-Perez, D., Taraborrelli, D., Sander, R., and Pozzer, A.: Global atmospheric budget of simple monocyclic aromatic compounds*, Atmos. Chem. Phys*., 16, 6931–6947, DOI: 10.5194/acp-16-6931-2016, 2016.

2. Sander, R.: Compilation of Henry's law constants (version 4.0) for water as solvent, *Atmos. Chem. Phys.*, 15, 4399–4981, DOI:10.5194/acp-15-4399-2015, 2015.

3. Mellouki, A., Ammann, M., Cox, R. A., Crowley, J. N., Herrmann, H., Jenkin, M. E., McNeill, V. F., Troe, J., and Wallington, T. J.: Evaluated kinetic and photochemical data for atmospheric chemistry: volume VIII – gas-phase reactions of organic species with four, or more, carbon atoms ($\geq C_4$), *Atmos. Chem. Phys*., 21, 4797–4808, DOI: 10.5194/acp-21-4797-2021, 2021.

4. Bloss, C., Wagner, V., Jenkin, M. E., Volkamer, R., Bloss, W. J., Lee, J. D., Heard, D. E., Wirtz, K., Martin-Reviejo, M., Rea, G., Wenger, J. C., and Pilling, M. J.: Development of a detailed chemical mechanism (MCMv3.1) for the atmospheric oxidation of aromatic hydrocarbons, *Atmos. Chem. Phys*., 5, 641–664, DOI: 10.5194/acp-5-641-2005, 2005.

5. Jenkin, M. E., Saunders, S. M., Wagner, V., and Pilling, M. J.: Protocol for the development of the Master Chemical Mechanism, MCM v3 (Part B): tropospheric degradation of aromatic volatile organic compounds, *Atmos. Chem. Phys*., 3, 181–193, DOI: 10.5194/acp-3-181-2003, 2003.

6. Schwantes, R. H., Schilling, K. A., McVay, R. C., Lignell, H., Coggon, M. M., Zhang, X., Wennberg, P. O., and Seinfeld, J. H.: Formation of highly oxygenated low-volatility products from cresol oxidation, *Atmos. Chem. Phys*., 17, 3453–3474, DOI: 10.5194/acp-17- 3453-2017, 2017.

7. Wallington, T. J., Ammann, M., Cox, R. A., Crowley, J. N., Herrmann, H., Jenkin, M. E., McNeill, V., Mellouki, A., Rossi, M. J., and Troe, J.: IUPAC Task group on atmospheric chemical kinetic data evaluation: Evaluated kinetic data, http://iupac.pole-ether.fr, 2018.

8. Roth, E., Chakir, A., and Ferhati, A.: Study of a benzoylperoxy radical in the gas phase: ultraviolet spectrum and $C_6H_5C(O)O_2 + HO_2$ reaction between 295 and 357 K, *J. Phys. Chem. A,* 114, 10 367–10 379, DOI: 10.1021/jp1021467, 2010.

9. Cabrera-Perez, D., Taraborrelli, D., Sander, R., and Pozzer, A.: Global atmospheric budget of simple monocyclic aromatic compounds, *Atmos. Chem. Phys*., 16, 6931–6947, DOI: 10.5194/acp-16-6931-2016, 2016.

10. Jagiella, S. and Zabel, F.: Reaction of phenylperoxy radicals with NO_2 at 298 K, *Phys. Chem. Chem. Phys.,* 9, 5036–5051, DOI: 10.1039/B705193J, 2007.

11. Tao, Z. and Li, Z.: A kinetics study on reactions of C_6H_5O with C_6H_5O and O_3 at 298 K, *Int. J. Chem. Kinet*., 31, 65–72, DOI: 10.1002/(SICI)1097-4601(1999)31:1<65::AID-KIN8>3.0.CO;2-J, 1999.

12. Platz, J., Nielsen, O. J., Wallington, T. J., Bali, J. C., Hurley, M. D., Straccia, A. M., Schneider, W. F., and Sehested, J.: Atmospheric chemistry of the phenoxy radical, $C_6H_5O(\bullet)$: UV spectrum and kinetics of its reaction with NO, NO_2, and O_2, *J. Phys. Chem. A*, 102 (41) 7964-7974, DOI: 10.1021/jp9822211, 1998.

13. Bejan, I., Abd El Aal, Y., Barnes, I., Benter, T., Bohn, B., Wiesen, P., and Kleffmann, J.: The photolysis of ortho-nitrophenols: a new gas phase source of HONO, *Phys. Chem. Chem. Phys*., 8, 2028–2035, DOI: 10.1039/B516590C, 2006.

14. Chen, J., Wenger, J. C., and Venables, D. S.: Near-ultraviolet absorption cross sections of nitrophenols and their potential influence on tropospheric oxidation capacity, *J. Phys. Chem. A*, 115, 12 235–12 242, DOI: 10.1021/jp206929r, 2011.

15. Newland, M. J., Rea, G. J., Thüner, L. P., Henderson, A. P., Golding, B. T., Rickard, A. R., Barnes, I., and Wenger, J.: Photochemistry of 2-butenedial and 4-oxo-2-pentenal under atmospheric boundary layer conditions, *Phys. Chem. Chem. Phys*., 21, 1160–1171, DOI: 10.1039/c8cp06437g, 2019.

16. Wang, S., Newland, M. J., Deng, W., Rickard, A. R., Hamilton, J. F., Muñoz, A., Rádenas, M., Vázquez, M. M., Wang, L., and Wang, X.: Aromatic Photo-oxidation, A New Source of Atmospheric Acidity, *Environ. Sci. Technol*., 54, 7798–7806, DOI: 10.1021/acs.est.0c00526, 2020.

17. Taraborrelli, D., Cabrera-Perez, D., Bacer, S., Gromov, S., Lelieveld, J., Sander, R., and Pozzer, A.: Influence of aromatics on tropospheric gas-phase composition, *Atmos. Chem. Phys.*, 21, 2615–2636, DOI: 10.5194/acp-21-2615-2021, 2021.

18. Porter, W. C., Safieddine, S. A., and Heald, C. L.: Impact of aromatics and monoterpenes on simulated tropospheric ozone and total OH reactivity. *Atmos. Environ.*, 169, 250-257, DOI: 10.1016/j.atmosenv.2017.08.048, 2017.

19. Fischer, E. V., Jacob, D. J., Yantosca, R. M., Sulprizio, M. P., Millet, D. B., Mao, J., Paulot, F., Singh, H. B., Roiger, A., Ries, L., Talbot, R. W., Dzepina, K., and Pandey Deolal, S.: Atmospheric peroxyacetyl nitrate (PAN): a global budget and source attribution, *Atmos. Chem. Phys.*, 14, 2679–2698, DOI: 10.5194/acp-14-2679-2014, 2014.

20. Hu, L., Millet, D. B., Baasandorj, M., Griffis, T. J., Travis, K. R., Tessum, C. W., Marshall, J. D., Reinhart, W. F., Mikoviny, T., Müller, M., Wisthaler, A., Graus, M., Warneke, C., and de Gouw, J.: Emissions of C_6–C_8 aromatic compounds in the United States: Constraints from tall tower and aircraft measurements, *J. Geophys. Res. Atmos.*, 120, 826– 842, DOI: 10.1002/2014JD022627, 2015.

Additional unnumbered references from figures S1-S2 (alphabetically):

Arey, J., Obermeyer, G., Aschmann, S. M., Chattopadhyay, S., Cusick, R. D., and Atkinson, R.: Dicarbonyl products of the OH radical-initiated reaction of a series of aromatic hydrocarbons, *Environ. Sci. Technol.*, 43, 683–689, DOI: 10.1021/es8019098, 2009.

Baltaretu, C. O., Lichtman, E. I., Hadler, A. B., and Elrod, M. J.: Primary atmospheric oxidation mechanism for toluene, *J. Phys. Chem. A,* 113, 221–230, DOI: 10.1021/jp806841t, 2009.

Berndt, T. and Böge, O.: Formation of phenol and carbonyls from the atmospheric reaction of OH radicals with benzene, *Phys. Chem. Chem. Phys.*, 8, 1205–1214, DOI: 10.1039/b514148f, 2006.

Berndt, T., Böge, O., and Herrmann, H.: On the formation of benzene oxide/oxepin in the gas-phase reaction of OH radicals with benzene, *Chem. Phys. Lett.*, 314, 435–442, DOI: 10.1016/S0009-2614(99)01041-6, 1999.

Birdsall, A. W. and Elrod, M. J.: Comprehensive NO-dependent study of the products of the oxidation of atmospherically relevant aromatic compounds*, J. Phys. Chem. A*, 115, 5397–5407, DOI: 10.1021/jp2010327, 2011.

Dumdei, B. E. and Kenny, D. V.: MS/MS analysis of the products of toluene photooxidation and measurement of their mutagenic activity, *Environ. Sci. Technol.,* 22, 1493–1498, DOI: 10.1021/es00177a017, 1988.

Gómez Alvarez, E., Viidanoja, J., Muñoz, A., Wirtz, K., and Hjorth, J.: Experimental confirmation of the dicarbonyl route in the photo- oxidation of toluene and benzene, *Environ. Sci. Technol.,* 41, 8362–8369, DOI: 10.1021/es0713274, 2007.

Ji, Y., Zhao, J., Terazono, H., Misawa, K., Levitt, N. P., Li, Y., Lin, Y., Peng, J., Wang, Y., Duan, L., Pan, B., Zhang, F., Feng, X., An, T., Marrero-Ortiz, W., Secrest, J., Zhang, A. L., Shibuya, K., Molina, M. J., and Zhang, R.: Reassessing the atmospheric oxidation mechanism of toluene, *Proc. Natl. Acad. Sci*., 114, 8169–8174, DOI: 10.1073/pnas.1705463114, 2017.

Klotz, B., Volkamer, R., Hurley, M. D., Sulbaek Andersen, M. P., Nielsen, O. J., Barnes, I., Imamura, T., Wirtz, K., Becker, K.-H., Platt, U., Wallington, T. J., and Washida, N.: OH-initiated oxidation of benzene. Part II. Influence of elevated NO_x concentrations, *Phys. Chem. Chem. Phys*., 4, 4399–4411, DOI: 10.1039/b204398j, 2002.

Wu, R., Pan, S., Li, Y., and Wang, L.: Atmospheric oxidation mechanism of toluene, *J. Phys. Chem. A,* 118, 4533–4547DOI: 10.1021/jp500077f, 2014.

Xu, L., Möller, K. H., Crounse, J. D., Kjaergaard, H. G., and Wennberg, P. O.: New Insights into the Radical Chemistry and Product Distribution in the OH-Initiated Oxidation of Benzene, *Environ. Sci. Technol*., 54, 13467–13477, DOI: 10.1021/acs.est.0c04780, 2020.

Zaytsev, A., Koss, A. R., Breitenlechner, M., Krechmer, J. E., Nihill, K. J., Lim, C. Y., Rowe, J. C., Cox, J. L., Moss, J., Roscioli, J. R., Canagaratna, M. R., Worsnop, D. R., Kroll, J. H., and Keutsch, F. N.: Mechanistic study of the formation of ring-retaining and ring- opening products from the oxidation of aromatic compounds under urban atmospheric conditions, *Atmos. Chem. Phys*., 19, 15 117–15 129, DOI: 10.5194/acp-19-15117-2019, 2019.